

Online Topology Identification from Vector Autoregressive Time Series

Bakht Zaman, *Student Member, IEEE*, Luis Miguel Lopez Ramos, *Member, IEEE*, Daniel Romero, *Member, IEEE*, and Baltasar Beferull-Lozano, *Senior Member, IEEE*

Abstract—Due to their capacity to condense the spatiotemporal structure of a data set in a format amenable for human interpretation, forecasting, and anomaly detection, causality graphs are routinely estimated in social sciences, natural sciences, and engineering. A popular approach to mathematically formalize causality is based on vector autoregressive (VAR) models, which constitutes an alternative to the well-known but usually intractable Granger causality. Relying on such a VAR causality notion, this paper develops two algorithms with complementary benefits to track time-varying causality graphs in an online fashion. Despite using data in a sequential fashion, both algorithms are shown to asymptotically attain the same average performance as a batch estimator with all data available at once. Moreover, their constant complexity per update renders these algorithms appealing for big-data scenarios. Theoretical and experimental performance analysis support the merits of the proposed algorithms. Remarkably, no probabilistic models or stationarity assumptions need to be introduced, which endows the developed algorithms with considerable generality.

I. INTRODUCTION

Inferring causal relations among time series finds countless applications in social sciences, natural sciences, and engineering. These relations are typically encoded as the edges of a causality graph, where each node corresponds to a time series, and oftentimes reveal the topology of e.g. an underlying social, biological, or brain network [2]. Causality graphs may also offer valuable insights into the spatiotemporal structure of time series and assist data processing tasks such as forecasting [3], signal reconstruction [4], anomaly detection [5], and dimensionality reduction [6]. But since causality graphs are seldom given, they must be inferred from time-series data.

Identifying graphs capturing the spatiotemporal “interactions” among time series has attracted great attention [2], [7]. Some approaches focus on instantaneous interactions, i.e., they disregard the temporal structure. The simplest is to place an edge between two nodes if the sample correlation between the associated time series exceeds a certain threshold [2]. To distinguish mediated from unmediated interactions [2, Sec. 7.3.2] one may resort to conditional independence, partial correlations, Markov random fields, or other approaches in graph signal processing; see e.g. [8]–[13]. To determine the direction of interactions, one may employ structural equation

models (SEM) [14] (see also [15] and references therein) or Bayesian networks [11]. However, all methods discussed so far account only for *memoryless* interactions, that is, they cannot accommodate delayed interactions where the values of a time series at a given time instant are related to the past values of another time series.

The earliest effort to formalize the notion of causality among time series is due to Granger [16] and relies on the rationale that *the cause precedes the effect*. A time series is said to be Granger-caused by another if the optimal prediction error of the former is decreased when the past of the latter is taken into account. Albeit elegant, this definition is generally impractical since the *optimal* prediction error is difficult to determine [17, p. 33], [18]. Thus, alternative causality definitions based on vector autoregressive (VAR) models are typically preferred [19]–[21]. VAR causality is determined from the support of VAR matrix parameters and is equivalent to Granger causality [22, Chap. 2] in certain cases (yet sometimes treated as equivalent [20], [21]). VAR causality is further motivated by the widespread usage of VAR models to approximate the response of systems of linear partial differential equations [23] and, more generally, in disciplines such as econometrics, bioinformatics, meteorology, neuroscience, and engineering [24]–[26]. VAR topologies are estimated assuming Gaussianity and stationarity in [27], [28] and assuming sparsity in [29]–[31].

All these approaches assume that the time series are stationary and, therefore, the associated graph does not change over time. Since this is not the case in most applications, other approaches have been devised to identify undirected time-varying topologies [32], [33] but, as all previously discussed approaches, their complexity becomes prohibitive for long observation windows since they process the entire data set at once and cannot accommodate data arriving sequentially. The modern approach to tackle these issues is *online* optimization, where an estimate is refined with every new data instance. Existing online topology identification from time series include [15], [34], which only account for memoryless interactions.

To sum up, except for methods that disregard temporal information, none of the aforementioned works estimate causality graphs in an online fashion. The only works accomplishing this task are the conference version [1] of the present paper and the more recent work [35]. The algorithm developed in the latter reference accommodates temporal structure but its computational complexity and memory requirements per iteration grow with the length of the time series.

The present paper fills this gap by developing two algorithms for online topology identification. Specifically, the

The work in this paper was supported by the SFI Offshore Mechatronics grant 237896/E30, the PETROMAKS Smart-Rig grant 244205 and the IKTPLUSS Indurb grant 270730/O70 from the Research Council of Norway.

The authors are with the WISENET Lab, Dept. of ICT, University of Agder, Jon Lilletunsvi 3, Grimstad, 4879 Norway. E-mails: {bakht.zaman, luismiguel.lopez, daniel.romero, baltasar.beferull}@uia.no.

The material in this work was presented, in part, at CAMSAP 2017 [1].

contributions are as follows: (C1) An online algorithm, termed *Topology Identification via Sparse Online learning* (TISO), which estimates directed VAR causality graphs and therefore captures memory in the interactions. Sparse and (possibly) time-varying topologies are tracked by a composite-objective iteration [36] that minimizes a sequential version of the criterion in [29] while promoting *sparse updates*. In addition, computational complexity and memory requirements per iteration remain constant, which renders the proposed algorithm suitable for sequential and big-data scenarios. (C2) A second algorithm, named *Topology Identification via Recursive Sparse Online learning* (TIRSO), which improves the tracking performance of TISO by minimizing a novel estimation criterion inspired by *recursive least squares* (RLS) where the instantaneous loss function accounts for past samples. TIRSO inherits the aforementioned benefits of TISO but incurs a moderate increase in computational complexity, which is still constant per iteration. (C3) The performance of TISO and TIRSO is theoretically analyzed by establishing sublinear growth of the relevant regret bounds. Hence, in the long run, these algorithms perform as well as the best (batch) predictor in hindsight, which supports their adoption for online topology identification. Remarkably, neither the algorithms nor the performance analysis require any probabilistic assumption, which endows the developed approaches with high generality. (C4) Finally, performance is also assessed empirically through extensive experiments with both synthetic and real data sets.

The rest of the paper is organized as follows: Sec. II presents the model, a batch estimation criterion, and background on online optimization. Sec. III develops TISO and TIRSO and establishes their asymptotic equivalence. Sec. IV and Sec. V analyze performance theoretically and by simulations, respectively. Sec. VI concludes the paper.

Notation: Bold lowercase (uppercase) letters denote column vectors (matrices). Operators $\mathbb{E}[\cdot]$, ∇ , $\bar{\nabla}$, $(\cdot)^\top$, $\text{vec}(\cdot)$, $\lambda_{\max}(\cdot)$, $\mathcal{R}(\cdot)$, $(\cdot)^\dagger$, and $\text{diag}(\cdot)$ respectively denote expectation, gradient, subgradient, matrix transpose, vectorization, maximum eigenvalue, range or column space, pseudo-inverse, and diagonal of a matrix. Symbols $\mathbf{0}_{N \times N}$ and $\mathbf{I}_{N \times N}$ respectively represent the all-zero matrix and the identity matrix of size $N \times N$. Moreover, $[\cdot]_+$ denotes $\max(\cdot, 0)$. For functions $f(x)$ and $g(x)$, the notation $f(x) \propto g(x)$ means that there exist two constants $a > 0$ and b such that $f(x) = ag(x) + b$. Finally, $\mathbb{1}$ is an indicator function satisfying $\mathbb{1}\{x\} = 0$ if $x = 0$ and $\mathbb{1}\{x\} = 1$ if $x \neq 0$.

II. PRELIMINARIES

After outlining the notion of directed causality graphs, this section reviews how these graphs can be identified in a batch fashion. Later, the basics of online optimization are described.

A. Directed Causality Graphs

Consider a collection of N time series, where $y_n[t]$, $t = 0, 1, \dots, T-1$, denotes the value of the n -th time series at time t . A causality graph $\mathcal{G} \triangleq (\mathcal{V}, \mathcal{E})$ is a graph where the n -th vertex in $\mathcal{V} = \{1, \dots, N\}$ is identified with the n -th time series $y_n[t]$ and there is an edge (or arc) from n' to n ($(n, n') \in \mathcal{E}$)

if and only if (iff) $y_{n'}[t]$ *causes* $y_n[t]$ according to a certain causality notion. For the reasons outlined in Sec. I, a prominent notion of causality can be defined using VAR models. To this end, consider the order- P VAR model

$$\mathbf{y}[t] = \sum_{p=1}^P \mathbf{A}_p \mathbf{y}[t-p] + \mathbf{u}[t], \quad (1)$$

where $\mathbf{y}[t] \triangleq [y_1[t], \dots, y_N[t]]^\top$, $\mathbf{A}_p \in \mathbb{R}^{N \times N}$, $p = 1, \dots, P$, are the matrices of VAR parameters, and $\mathbf{u}[t] \triangleq [u_1[t], \dots, u_N[t]]^\top$ is the *innovation process*, generally assumed to be a white zero-mean stochastic process, i.e., $\mathbb{E}[\mathbf{u}[t]] = \mathbf{0}$ and $\mathbb{E}[\mathbf{u}[t]\mathbf{u}^\top[\tau]] = \mathbf{0}_{N \times N}$ for $t \neq \tau$. Yet, the present work needs no such assumptions. With $a_{n,n'}^{(p)}$ the n, n' -th entry of \mathbf{A}_p , (1) takes the following form

$$\begin{aligned} y_n[t] &= \sum_{n'=1}^N \sum_{p=1}^P a_{n,n'}^{(p)} y_{n'}[t-p] + u_n[t] \\ &= \sum_{n' \in \mathcal{N}(n)} \sum_{p=1}^P a_{n,n'}^{(p)} y_{n'}[t-p] + u_n[t], \end{aligned} \quad (2)$$

for $n = 1, \dots, N$, where $\mathcal{N}(n) \triangleq \{n' : \mathbf{a}_{n,n'} \neq \mathbf{0}\}$ and $\mathbf{a}_{n,n'} \triangleq [a_{n,n'}^{(1)}, \dots, a_{n,n'}^{(P)}]^\top$. Recognizing the convolution operation in the right-hand side enables one to express (2) as $y_n[t] = \sum_{n' \in \mathcal{N}(n)} a_{n,n'}^{(t)} * y_{n'}[t] + u_n[t]$ in signal processing notation. Thus, in a VAR model, $y_n[t]$ equals the sum of noise and the output of $|\mathcal{N}(n)|$ linear time-invariant filters.

When $\mathbf{u}[t]$ is a zero-mean and temporally white stochastic process, the term $\hat{y}_n[t] \triangleq \sum_{n' \in \mathcal{N}(n)} \sum_{p=1}^P a_{n,n'}^{(p)} y_{n'}[t-p]$ in (2) is the *minimum mean square error estimator* of $y_n[t]$ given the previous values of all time series $\{y_{n'}[\tau], n' = 1, \dots, N, \tau < t\}$; see e.g. [18, Sec. 12.7]. The set $\mathcal{N}(n)$ therefore collects the indices of those time series that participate in this optimal predictor of $y_n[t]$ or, alternatively, the information provided by time series $y_{n'}[t]$ with $n' \notin \mathcal{N}(n)$ is not informative to predict $y_n[t]$. This motivates the following definition of causality: $y_{n'}[t]$ *VAR-causes* $y_n[t]$ whenever $n' \in \mathcal{N}(n)$. Equivalently, $y_{n'}[t]$ *VAR-causes* $y_n[t]$ if $\mathbf{a}_{n,n'} \neq \mathbf{0}$. VAR causality¹ relations among the N time series can be represented using a causality graph where $\mathcal{E} \triangleq \{(n, n') : \mathbf{a}_{n,n'} \neq \mathbf{0}\}$. Clearly, in such a graph, $\mathcal{N}(n)$ is the in-neighborhood of node n . To quantify the strength of these causality relations, a weighted graph can be constructed by assigning e.g. the weight $\|\mathbf{a}_{n,n'}\|_2$ to the edge (n, n') .

With these definitions, the *batch* problem of identifying a VAR causality graph reduces to estimating the VAR coefficient matrices $\{\mathbf{A}_p\}_{p=1}^P$ given P and the observations $\{\mathbf{y}[t]\}_{t=0}^{T-1}$. To simplify notation, form the tensor \mathcal{A} by stacking the matrices $\{\mathbf{A}_p\}_{p=1}^P$ along the third dimension.

B. Batch Estimation Criterion for Topology Identification

This section presents an estimation criterion that can be used to address the batch estimation problem formulated in

¹A detailed comparison with Granger causality lies out of scope, but it is worth mentioning that the main distinction lies in the prediction horizon: whereas VAR causality just pertains to prediction 1 time instant ahead, Granger causality involves prediction of all future samples $y_n[t']$, $t' \geq t$, given the ones up to a certain time instant $\{y_{n'}[\tau], n' = 1, \dots, N, \tau < t\}$. Therefore VAR causality implies Granger causality, but the converse is false. See [22, Sec. 2.3.1] for a more detailed comparison.

Sec. II-A. The most immediate approach would be to pursue a *least-squares* estimate by minimizing the loss [22]

$$\begin{aligned} \mathcal{L}(\mathcal{A}) &\triangleq \frac{1}{2(T-P)} \sum_{\tau=P}^{T-1} \left\| \mathbf{y}[\tau] - \sum_{p=1}^P \mathbf{A}_p \mathbf{y}[\tau-p] \right\|_2^2 \\ &= \frac{1}{2(T-P)} \sum_{n=1}^N \sum_{\tau=P}^{T-1} \left[y_n[\tau] - \sum_{n'=1}^N \sum_{p=1}^P a_{n,n'}^{(p)} y_{n'}[\tau-p] \right]^2. \end{aligned}$$

This estimation task becomes undetermined unless the number NT of available data samples meaningfully exceeds the number of unknowns PN^2 . To circumvent this limitation, the following criterion has been proposed in [29]:

$$\arg \min_{\mathcal{A}} \mathcal{L}(\mathcal{A}) + \lambda \sum_{n=1}^N \sum_{n'=1, n' \neq n}^N \|\mathbf{a}_{n,n'}\|_2, \quad (3)$$

where $\lambda > 0$ is a regularization parameter that can be adjusted e.g., via cross-validation [11, Chap. 1]. The second term in (3) is conventionally referred to as a *group-lasso* regularizer and the solution to (3) as a *group-lasso* estimate [37]. This promotes a *group-sparse structure* in $\{\mathbf{A}_p\}_{p=1}^P$ to exploit the information that the number of edges in \mathcal{E} is typically small. Self-connections $(\mathbf{a}_{n,n}, n = 1, \dots, N)$ are excluded from the regularization term so that the inferred causal relations pertain to the component of each time series that cannot be predicted using its own past [29].

Remarkably, (3) separates along n . To see this, let $\mathbf{a}_n \triangleq [\mathbf{a}_{n,1}^\top, \mathbf{a}_{n,2}^\top, \dots, \mathbf{a}_{n,N}^\top]^\top \in \mathbb{R}^{NP}$ and

$$\mathbf{g}[t] \triangleq \text{vec}([\mathbf{y}[t-1], \dots, \mathbf{y}[t-P]]^\top) \in \mathbb{R}^{NP}, \quad (4)$$

and express $\mathcal{L}(\mathcal{A})$ as $\mathcal{L}(\mathcal{A}) = \sum_{n=1}^N \ell^{(n)}(\mathbf{a}_n)$, where $\ell^{(n)}(\mathbf{a}_n) \triangleq (1/(T-P)) \sum_{t=P}^{T-1} \ell_t^{(n)}(\mathbf{a}_n)$ and $\ell_t^{(n)}(\mathbf{a}_n) \triangleq (1/2)(y_n[t] - \mathbf{g}^\top[t] \mathbf{a}_n)^2$. Then, (3) becomes $\{\mathbf{a}_n^*\}_{n=1}^N = \arg \min_{\{\mathbf{a}_n\}_{n=1}^N} \sum_{n=1}^N [\ell^{(n)}(\mathbf{a}_n) + \lambda \sum_{n'=1, n' \neq n}^N \|\mathbf{a}_{n,n'}\|_2]$, which can be solved by separately solving N subproblems of the form

$$\mathbf{a}_n^* = \arg \min_{\mathbf{a}_n} \ell^{(n)}(\mathbf{a}_n) + \lambda \sum_{n'=1, n' \neq n}^N \|\mathbf{a}_{n,n'}\|_2. \quad (5)$$

Hence, the VAR causality graph can be identified by separately estimating the incoming edges for each node, which for the n -th node are found through (5).

The batch estimation criterion in (5) requires all data $\{\mathbf{y}[t]\}_{t=0}^{T-1}$ before an estimate can be obtained. Furthermore, the complexity of solving (5) eventually becomes prohibitive for sufficiently large T . To tackle these difficulties, this paper adopts the framework of online optimization, reviewed next.

C. Background on Online Optimization

This section reviews the fundamental notions of online optimization from a general perspective, not necessarily applied to the problem of topology identification. To this end, consider the generic unconstrained optimization problem

$$\text{minimize}_{\mathbf{a}} \frac{1}{T_0} \sum_{t=0}^{T_0-1} h_t(\mathbf{a}), \quad (6)$$

where $h_t(\mathbf{a})$ is a convex function that in many applications depends on the data received at time t . For example, in least

squares $h_t(\mathbf{a}) = \|\mathbf{X}_t \mathbf{a} - \mathbf{y}[t]\|_2^2$, where $\mathbf{y}[t]$ is the data vector received at time t and \mathbf{X}_t is a given matrix. To solve (6), it is necessary that all $\{h_t(\mathbf{a})\}_{t=0}^{T_0-1}$ be available. Approaches that process all data at once are termed *batch* and, hence, suffer from potentially long waiting times, which generally render them inappropriate for real-time operation. Besides, computational complexity and memory generally grow super-linearly with T_0 , which eventually becomes prohibitive.

Online algorithms alleviate these limitations. They compute a new $\mathbf{a}[t+1]$ every time a new $\mathbf{y}[t]$ (or, more generally, a new $h_t(\mathbf{a})$) is processed. At every iteration, also known as *update*, $\mathbf{a}[t+1]$ is obtained from $\mathbf{a}[t]$, $\mathbf{y}[t]$, and possibly some additional information carried from each update to the next. The memory requirements and number of arithmetic operations per iteration must not grow unbounded for increasing t . Thus, online algorithms are especially appealing when data vectors are received sequentially or T_0 is so large that batch solvers are not affordable. Additionally, online algorithms can track changes in the underlying model.

The most common performance metric to evaluate online algorithms is the *regret*, which quantifies the cumulative loss incurred by an online algorithm relative to the optimal constant solution in hindsight. Formally, the regret at iteration $T_0 - 1$ is given by [38]:

$$R(T_0) \triangleq \sum_{t=0}^{T_0-1} [h_t(\mathbf{a}[t]) - h_t(\mathbf{a}^*[T_0])], \quad (7)$$

where $\mathbf{a}^*[T_0] \triangleq \arg \min_{\mathbf{a}} (1/T_0) \sum_{t=0}^{T_0-1} h_t(\mathbf{a})$ is the optimal *constant* hindsight solution, i.e., the batch solution after T_0 data vectors have been processed. To be deemed admissible, online algorithms must yield a *sublinear regret*, i.e., $R(T_0)/T_0 \rightarrow 0$ as $T_0 \rightarrow \infty$. If this condition is satisfied, then the online algorithm performs asymptotically as well as the batch solution *on average*.

Arguably the simplest online optimization method is *online (sub)gradient descent* (OGD/OSGD), which obtains $\mathbf{a}[t+1] = \mathbf{a}[t] - \alpha_t \tilde{\nabla} h_t(\mathbf{a}[t])$ with $\alpha_t > 0$ the step size. The regret of OSGD is sublinear under broad conditions [38, Corollary 2.7].

III. ONLINE TOPOLOGY IDENTIFICATION

This section develops online algorithms to solve (5). To this end, one can cast (5) in the form (6) by setting

$$h_t(\mathbf{a}_n) = \ell_{t+P}^{(n)}(\mathbf{a}_n) + \lambda \sum_{n'=1, n' \neq n}^N \|\mathbf{a}_{n,n'}\|_2, \quad (8)$$

for $t = 0, \dots, T - P - 1$. The most immediate approach to solve (8) is to apply OSGD, in which case the update is given by $\mathbf{a}_n[t+1] = \mathbf{a}_n[t] - \alpha_t \tilde{\mathbf{w}}_n[t]$ with $\tilde{\mathbf{w}}_n[t]$ a subgradient of h_t at $\mathbf{a}_n[t]$. Clearly, $\tilde{\mathbf{w}}_n[t]$ equals $\nabla \ell_{t+P}^{(n)}(\mathbf{a}_n[t])$ plus a valid subgradient of $\sum_{n'=1, n' \neq n}^N \|\mathbf{a}_{n,n'}\|_2$. Such a subgradient can be obtained by evaluating

$$\begin{aligned} \tilde{\nabla}_{\mathbf{a}_n} \sum_{\substack{n'=1 \\ n' \neq n}}^N \|\mathbf{a}_{n,n'}\|_2 &\triangleq [\tilde{\nabla}_{\mathbf{a}_{n,1}}^\top \|\mathbf{a}_{n,1}\|_2, \dots, \tilde{\nabla}_{\mathbf{a}_{n,n-1}}^\top \|\mathbf{a}_{n,n-1}\|_2, \\ &\mathbf{0}, \tilde{\nabla}_{\mathbf{a}_{n,n+1}}^\top \|\mathbf{a}_{n,n+1}\|_2, \dots, \tilde{\nabla}_{\mathbf{a}_{n,N}}^\top \|\mathbf{a}_{n,N}\|_2]^\top, \quad (9) \end{aligned}$$

at $\mathbf{a}_n = \mathbf{a}_n[t]$, where $\tilde{\nabla}_{\mathbf{x}} \|\mathbf{x}\|_2 = \frac{\mathbf{x}}{\|\mathbf{x}\|_2}$, for $\mathbf{x} \neq \mathbf{0}$ and $\tilde{\nabla}_{\mathbf{x}} \|\mathbf{x}\|_2 = \mathbf{0}$, for $\mathbf{x} = \mathbf{0}$. Since $\nabla \ell_{t+P}^{(n)}(\mathbf{a}_n[t])$ is not necessarily sparse, it follows from the update equation that

the iterates $\mathbf{a}_n[t]$ before convergence are not sparse in general. Since the optimal $\mathbf{a}[t]$, which is the solution to the batch problem at time t , is actually sparse, this observation calls for alternative approaches that produce sparse iterates.

To this end, note that the reason behind the failure of OSGD to provide sparse iterates is that this algorithm implicitly linearizes the entire instantaneous objective $h_t(\mathbf{a})$. Since the regularizer is non-differentiable, it is not well approximated by a linear function and, as a result, it fails to promote sparsity. To circumvent this limitation, *composite* algorithms decompose $h_t(\mathbf{a})$ as $h_t(\mathbf{a}) = f_t(\mathbf{a}) + \Omega(\mathbf{a})$, where $f_t(\mathbf{a})$ is a convex loss function and $\Omega(\mathbf{a})$ is a convex regularizer, and linearize only $f_t(\mathbf{a})$. Algorithms of this family, which include *regularized dual averaging* [39] and *composite objective mirror descent* (COMID) [36], solve the generic problem

$$\underset{\mathbf{a}}{\text{minimize}} \frac{1}{T_0} \sum_{t=0}^{T_0-1} [f_t(\mathbf{a}) + \Omega(\mathbf{a})]. \quad (10)$$

without linearizing $\Omega(\mathbf{a})$. Instead, $\Omega(\mathbf{a})$ is utilized at every iteration to produce sparse updates. For instance, the COMID update is given by

$$\begin{aligned} \mathbf{a}[t+1] = & \underset{\mathbf{a}}{\text{arg min}} \tilde{\nabla} f_t^\top(\mathbf{a}[t]) (\mathbf{a} - \mathbf{a}[t]) \\ & + \frac{1}{\alpha_t} B_\psi(\mathbf{a}, \mathbf{a}[t]) + \Omega(\mathbf{a}), \end{aligned} \quad (11)$$

where $\tilde{\nabla} f_t(\mathbf{a}[t])$ is a subgradient of f_t at point $\mathbf{a}[t]$, $\alpha_t > 0$ is a step size, and

$$B_\psi(\mathbf{w}, \mathbf{v}) \triangleq \psi(\mathbf{w}) - \psi(\mathbf{v}) - \nabla \psi^\top(\mathbf{v})(\mathbf{w} - \mathbf{v}), \quad (12)$$

is the so-called Bregman divergence associated with a ζ -strongly convex and continuously differentiable function ψ . The strong convexity condition means that $B_\psi(\mathbf{w}, \mathbf{v}) \geq (\zeta/2)\|\mathbf{w} - \mathbf{v}\|^2$, which motivates using $B_\psi(\mathbf{w}, \mathbf{v})$ as a surrogate of a distance between \mathbf{w} and \mathbf{v} . Thus, the Bregman divergence in (11) penalizes updates $\mathbf{a}[t+1]$ lying far from the previous one $\mathbf{a}[t]$, which essentially smoothes the sequence of iterates. Relative to each term in (10), the loss f_t in (11) has been linearized but the regularizer $\Omega(\mathbf{a})$ has been kept intact. When $\Omega(\mathbf{a})$ is a sparsity-promoting regularizer, then $\mathbf{a}[t+1]$ is therefore expected to be sparse.

In view of these appealing features, the algorithm proposed in Sec. III-A builds upon COMID to address the problem of online causality graph identification.

A. Topology Identification via Sparse Online optimization (TISO)

This section proposes *topology identification via sparse online optimization* (TISO), an online algorithm that provides a causality graph estimate every time a new data vector $\mathbf{y}[t]$ is processed. The key idea of this first algorithm is to refine the previous topology estimate with the information provided by the new data vector by means of a COMID update.

To this end, it is required to (i) properly decompose the objective into a function that is linearized plus a function that is not, and (ii) choose a suitable Bregman divergence so that the COMID update has a closed form. In this section, step

(i) is accomplished by decomposing the h_t in (8) as $h_t(\mathbf{a}) = f_t(\mathbf{a}) + \Omega(\mathbf{a})$ with

$$f_t(\mathbf{a}_n) = \ell_{t+P}^{(n)}(\mathbf{a}_n), \quad (13a)$$

$$\Omega(\mathbf{a}_n) = \lambda \sum_{n'=1, n' \neq n}^N \|\mathbf{a}_{n,n'}\|_2, \quad (13b)$$

for $t = 0, \dots, T - P - 1$. In the next section, a more sophisticated decomposition will be adopted to improve convergence and increase the ability to track changes in the causality graph. Regarding (ii), it will be seen that the COMID objective in (11) with $\Omega(\mathbf{a}_n)$ given by (13b) can be solved in closed form when B_ψ is the Bregman divergence associated with $\psi(\cdot) = \frac{1}{2}\|\cdot\|_2^2$, since in that case B_ψ becomes $B_\psi(\mathbf{w}, \mathbf{v}) = \frac{1}{2}\|\mathbf{w} - \mathbf{v}\|_2^2$ and $\mathbf{a}[t+1]$ can be found via *group soft-thresholding*, as detailed next. With these expressions, the TISO update reads as

$$\mathbf{a}_n[t+1] = \underset{\mathbf{a}_n}{\text{arg min}} J(\mathbf{a}_n), \quad (14)$$

where $\mathbf{a}_n[t+1]$ is the topology estimate after $\{\mathbf{y}[\tau]\}_{\tau=0}^t$ have been processed and

$$\begin{aligned} J(\mathbf{a}_n) \triangleq & \mathbf{v}_n^\top[t] (\mathbf{a}_n - \mathbf{a}_n[t]) + \frac{1}{2\alpha_t} \|\mathbf{a}_n - \mathbf{a}_n[t]\|_2^2 \\ & + \lambda \sum_{n'=1, n' \neq n}^N \|\mathbf{a}_{n,n'}\|_2. \end{aligned} \quad (15)$$

To obtain the subgradient $\mathbf{v}_n[t]$, recall that $\ell_t^{(n)}(\mathbf{a}_n) \triangleq (1/2)(y_n[t] - \mathbf{g}^\top[t] \mathbf{a}_n)^2$ to find that

$$\mathbf{v}_n[t] \triangleq \nabla \ell_t^{(n)}(\mathbf{a}_n[t]) = \mathbf{g}[t] (\mathbf{g}^\top[t] \mathbf{a}_n[t] - y_n[t]). \quad (16)$$

The minimization problem in (14) will be solved next in closed form. To this end, expand the squared norm and ignore the constants to obtain

$$\begin{aligned} J(\mathbf{a}_n) \propto & \frac{\mathbf{a}_n^\top \mathbf{a}_n}{2\alpha_t} + \mathbf{a}_n^\top (\mathbf{v}_n[t] - \frac{1}{\alpha_t} \mathbf{a}_n[t]) + \lambda \sum_{n'=1, n' \neq n}^N \|\mathbf{a}_{n,n'}\|_2 \\ = & \sum_{n'=1}^N \left[\frac{1}{2\alpha_t} \mathbf{a}_{n,n'}^\top \mathbf{a}_{n,n'} + \mathbf{a}_{n,n'}^\top (\mathbf{v}_{n,n'}[t] - \frac{1}{\alpha_t} \mathbf{a}_{n,n'}[t]) \right. \\ & \left. + \lambda \|\mathbf{a}_{n,n'}\|_2 \mathbb{1}\{n' \neq n\} \right], \end{aligned} \quad (17)$$

where $\mathbf{v}_{n,n'}[t] \in \mathbb{R}^P$ is the n' -th subvector of $\mathbf{v}_n[t]$, i.e., $\mathbf{v}_n[t] \triangleq [\mathbf{v}_{n,1}^\top[t], \dots, \mathbf{v}_{n,N}^\top[t]]^\top$. From (17), it can be observed that the problem of minimizing $J(\mathbf{a}_n)$ can be separated along the groups $n' = 1, \dots, N$.

For $n' \neq n$, the n' -th subvector of $\mathbf{a}_n[t+1]$ (or n' -th *group*) can be expressed in terms of the so-called multidimensional shrinkage-thresholding operator [40] as:

$$\mathbf{a}_{n,n'}[t+1] = \mathbf{a}_{n,n'}^f[t] \left[1 - \frac{\alpha_t \lambda}{\|\mathbf{a}_{n,n'}^f[t]\|_2} \right]_+, \quad (18)$$

where $\mathbf{a}_{n,n'}^f[t] \triangleq \mathbf{a}_{n,n'}[t] - \alpha_t \mathbf{v}_{n,n'}[t]$. Expression (18) is composed of two terms: whereas $\mathbf{a}_{n,n'}^f[t]$ is the result of performing a gradient-descent step in a direction that decreases the instantaneous loss $\ell_t^{(n)}(\mathbf{a}_n)$, the second term promotes *group sparsity* by setting $\mathbf{a}_{n,n'}[t+1] = \mathbf{0}$ for those groups n' with $\|\mathbf{a}_{n,n'}^f[t]\|_2 \leq \alpha_t \lambda$. Recalling that each vector $\mathbf{a}_{n,n'}$ corresponds to an edge in the estimated causality graph (see Sec. II-A), expression (18) indicates that only the relatively

strong edges (i.e. causality relations) survive. As intuition predicts given the role of λ as the regularization parameter scaling a sparsity-promoting term in (3), condition $\|\mathbf{a}_{n,n'}^f[t]\|_2 \leq \alpha_t \lambda$ indicates that the greater λ , the sparser the estimated graph.

On the other hand, when $n' = n$, the n' -th subvector of $\mathbf{a}_n[t+1]$ in (14) is given by:

$$\mathbf{a}_{n,n'}[t+1] = \mathbf{a}_{n,n'}[t] - \alpha_t \mathbf{v}_{n,n'}[t] = \mathbf{a}_{n,n'}^f[t] \quad (19)$$

and, as intended, no sparsity is promoted on self-connections; see Sec. II-B. Combining (18) and (19), the estimate of the n' -th group at time $t+1$ is given by:

$$\mathbf{a}_{n,n'}[t+1] = \mathbf{a}_{n,n'}^f[t] \left[1 - \frac{\alpha_t \lambda \mathbf{1}_{\{n \neq n'\}}}{\|\mathbf{a}_{n,n'}^f[t]\|_2} \right]_+ \quad (20)$$

The performance of TISO depends on the choice of the step-size sequence $\{\alpha_t\}_t$. Three possibilities include (i) constant stepsize, attractive for non-stationary setups where changes in the coefficients \mathcal{A} need to be tracked over time; (ii) diminishing stepsize, commonly in the form of $\mathcal{O}(1/t)$ or $\mathcal{O}(1/\sqrt{t})$, which provides performance guarantees under a certain probabilistic model for the data [36, Sec. 6]; or (iii) an adaptive stepsize that depends on the data, as explored in Sec. V. The overall TISO algorithm is listed as **Procedure 1**. In terms of memory, TISO requires only storing the last P data vectors and the last estimate, resulting in $\mathcal{O}(N^2P)$ memory complexity. On the other hand, each estimate update requires $\mathcal{O}(N^2P)$ arithmetic operations, and the total number of entries of \mathcal{A} to be estimated is precisely N^2P . Thus, TISO can arguably be deemed a low-complexity algorithm.

One can establish links between TISO and other algorithms in the literature. For instance, TISO would coincide with the popular *least mean squares* (LMS) algorithm when $\lambda = 0$ and therefore no group sparsity is promoted. If, beyond the application of online topology identification, one wishes to see TISO as an online algorithm to solve certain instances of the group lasso problems, then TISO is related to the algorithm in [41] applied to group lasso. However, this algorithm does not produce sparse iterates and its convergence has not been established analytically. TISO is also related to the algorithm in [42], obtained by applying regularized dual averaging (RDA) [39] to a group lasso objective. The benefits of TISO relative to this algorithm are therefore the benefits of COMID over RDA [36], [39]. Finally, another related algorithm is [43], which operates in an online fashion but is confined to groups of size one.

Before delving into analyzing convergence of TISO in Sec. IV, the next section will build upon TISO to develop an algorithm with increased robustness to noise.

B. Topology Identification via *Recursive Sparse Online optimization* (TIRSO)

As seen in Sec. III-A, each update of TISO depends on the data through the *instantaneous* loss $\ell_t^{(n)}(\mathbf{a}_n[t]) \triangleq (1/2)(y_n[t] - \mathbf{g}^\top[t] \mathbf{a}_n[t])^2$, which quantifies the prediction error of the newly received vector $\mathbf{y}[t]$ when the VAR parameters \mathcal{A} are given by the previous estimate $\mathbf{a}_n[t]$. Thus, the residual of predicting each data vector is used only in a single

Procedure 1 Topology Identification via Sparse Online optimization (TISO)

Input: $P, \lambda, \{\alpha_t\}_t, \{\mathbf{y}[\tau]\}_{\tau=0}^{P-1}$

Output: $\{\mathbf{a}_n[\tau]\}_{n=1}^N, \tau = P, P+1, \dots$

Initialization: $\mathbf{a}_n[P] = \mathbf{0}, n = 1, \dots, N$

```

1: for  $t = P, P+1, \dots$  do
2:   Receive data vector  $\mathbf{y}[t]$ 
3:   Form  $\mathbf{g}[t]$  via (4)
4:   for  $n = 1, 2, \dots, N$  do
5:      $\mathbf{v}_n[t] = (\mathbf{g}^\top[t] \mathbf{a}_n[t] - y_n[t])\mathbf{g}[t]$ 
6:     for  $n' = 1, 2, \dots, N$  do
7:        $\mathbf{a}_{n,n'}^f[t] = \mathbf{a}_{n,n'}[t] - \alpha_t \mathbf{v}_{n,n'}[t]$ 
8:       Compute  $\mathbf{a}_{n,n'}[t+1]$  via (20)
9:     end for
10:  end for
11: end for

```

TISO update. Although this renders TISO a computationally efficient algorithm for identifying (possibly time-varying) topologies in an online fashion, it also increases sensitivity to noise and input variability. This section pursues an alternative approach targeted to alleviate this sensitivity at the expense of a moderate increase in computational complexity and memory requirements.

It is clear from (15) that each update of TISO is determined by the previous estimate $\mathbf{a}_n[t]$ and by $\mathbf{v}_n[t]$, which incorporates the residual only at time t . The step-size α_t controls how much variability in the input data propagates to the estimates $\mathbf{a}_n[t]$ since the second term in the right-hand side promotes estimates that deviate less from the previous estimate $\mathbf{a}_n[t]$. When a diminishing step size sequence is adopted, the influence of each new $\mathbf{y}[t]$ on the estimate becomes arbitrarily small, and estimate variability fades away. However, these sequences cannot be utilized when the application at hand demands tracking changes in the topology or coefficients \mathcal{A} . In these settings, a constant (or adaptive, as discussed in Sec. IV) step size sequence is preferable. In such a scenario, a desire to reduce output variability would prompt the adoption of small step sizes $\alpha_t = \alpha$. However, this would slow down convergence, which would hinder the ability of TISO to track changes in the VAR coefficients \mathbf{a}_n . Since many real-world processes remain stationary only for limited intervals of time, the VAR coefficients \mathcal{A} may change before the algorithm has converged if a small α is adopted.

An alternative approach to reduce output variability will be developed next by drawing inspiration from the connections between TISO and the classical LMS and *recursive least squares* (RLS) algorithms used in signal processing. Indeed, as mentioned in Sec. III-A, TISO generalizes LMS, which is recovered for $\lambda = 0$. To speed up convergence and reduce variability in the output of LMS, it is customary to resort to RLS, which accommodates the received data in a more sophisticated fashion, allowing furthermore to control the influence of each data vector on future estimates through forgetting factors.

To proceed along these lines, the trick here will be to

replace the *instantaneous* loss $\ell_t^{(n)}(\mathbf{a}_n)$ in (13) with a *running average* loss. To maintain tracking capabilities, a heavier weight is assigned recent data using the exponential window customarily adopted by RLS. Specifically, consider setting $f_t(\mathbf{a}_n) = \tilde{\ell}_t^{(n)}(\mathbf{a}_n)$ in (13) with

$$\tilde{\ell}_t^{(n)}(\mathbf{a}_n) \triangleq \mu \sum_{\tau=P}^t \gamma^{t-\tau} \ell_\tau^{(n)}(\mathbf{a}_n), \quad (21)$$

where $\gamma \in (0, 1)$ is the user-selected forgetting factor and $\mu > 0$ is a scaling constant which, unless otherwise stated, will be set to the value $\mu = 1 - \gamma$ that normalizes the exponential weighting window, i.e., $\mu \sum_{\tau=0}^{\infty} \gamma^\tau = 1$. Note that, with this selection of $f_t(\mathbf{a}_n)$, the associated objective (10) no longer equals the batch estimation criterion in (5), but both asymptotically coincide; see Theorem 1.

Having specified a loss function, the next step is to derive the update equation. In a direct application of COMID to solve (10) with $f_t(\mathbf{a}_n) = \tilde{\ell}_t^{(n)}(\mathbf{a}_n)$, each iteration would involve the evaluation of the gradient of the $t - P + 1$ terms of $\tilde{\ell}_t^{(n)}$. The computational complexity per iteration would grow with t and, therefore, the resulting updates would not make up an online algorithm; see Sec. II-C. To remedy this issue, the structure of (21) will be exploited next to develop an algorithm with constant memory and complexity per iteration. To this end, expand and rewrite (21) to obtain

$$\begin{aligned} \tilde{\ell}_t^{(n)}(\mathbf{a}_n) &= \frac{\mu}{2} \sum_{\tau=P}^t \gamma^{t-\tau} (y_n^2[t] + \mathbf{a}_n^\top \mathbf{g}[t] \mathbf{g}^\top[t] \mathbf{a}_n \\ &\quad - 2y_n[t] \mathbf{g}^\top[t] \mathbf{a}_n) \\ &= \frac{1}{2} \mathbf{a}_n^\top \Phi[t] \mathbf{a}_n - \mathbf{r}_n^\top[t] \mathbf{a}_n + \frac{\mu}{2} \sum_{\tau=P}^t \gamma^{t-\tau} y_n^2[t], \end{aligned} \quad (22)$$

where

$$\Phi[t] \triangleq \mu \sum_{\tau=P}^t \gamma^{t-\tau} \mathbf{g}[\tau] \mathbf{g}^\top[\tau], \quad (23)$$

and $\mathbf{r}_n[t] \triangleq \mu \sum_{\tau=P}^t \gamma^{t-\tau} y_n[\tau] \mathbf{g}[\tau]$, can be respectively thought of as a weighted sample autocorrelation matrix and a weighted sample cross-correlation vector. The key observation here is that, as occurs in RLS, these quantities can be updated recursively as $\Phi[t] = \gamma \Phi[t-1] + \mu \mathbf{g}[t] \mathbf{g}^\top[t]$ and $\mathbf{r}_n[t] = \gamma \mathbf{r}_n[t-1] + \mu y_n[t] \mathbf{g}[t]$. Noting that $\nabla \tilde{\ell}_t^{(n)}(\mathbf{a}_n) = \Phi[t] \mathbf{a}_n - \mathbf{r}_n[t]$, defining $\tilde{\mathbf{v}}_n[t] \triangleq [\tilde{\mathbf{v}}_{n,1}^\top[t], \dots, \tilde{\mathbf{v}}_{n,N}^\top[t]]^\top \triangleq \nabla \tilde{\ell}_t^{(n)}(\mathbf{a}_n[t])$ and proceeding similarly to Sec. III-A yields the update

$$\tilde{\mathbf{a}}_{n,n'}[t+1] = \tilde{\mathbf{a}}_{n,n'}^f[t] \left[1 - \frac{\alpha_t \lambda \mathbb{1}\{n \neq n'\}}{\|\tilde{\mathbf{a}}_{n,n'}^f[t]\|_2} \right]_+, \quad (24)$$

where $\tilde{\mathbf{a}}_{n,n'}^f[t] \triangleq \tilde{\mathbf{a}}_{n,n'}[t] - \alpha_t \tilde{\mathbf{v}}_{n,n'}[t]$. Despite involving different quantities, this expression has the same structure as (20) and therefore the same remarks on interpretation and step-size selection in Sec. III-A still apply.

Due to the recursive nature of the updates for $\Phi[t]$ and $\mathbf{r}_n[t]$, the resulting algorithm is termed *Topology Identification via Recursive Sparse Online optimization* (TIRSO) and tabulated as **Procedure 2**. Observe that $\Phi[t]$ only needs to be updated once per observed sample t , whereas N vectors $\{\mathbf{r}_n[t]\}_{n=1}^N$ need to be updated at every t . The computational complexity is dominated by step 7, which involves $\mathcal{O}(N^3 P^2)$ operations per t . However, the group-sparse structure of $\tilde{\mathbf{a}}_n$ helps to reduce the computation. For instance, if the graph has $\mathcal{O}(N)$ edges, then it can be easily seen that complexity is still dominated

by step 7 but this step requires only $\mathcal{O}(N^2 P^2)$ operations per t . Regarding memory complexity, TIRSO requires $N^2 P^2$ memory positions to store $\Phi[t]$ and $N^2 P$ positions to store $\{\mathbf{r}_n[t]\}_{n=1}^N$.

Procedure 2 Topology Identification via Recursive Sparse Online optimization (TIRSO)

Input: $\gamma, \mu, P, \lambda, \sigma^2, \{\alpha_t\}_t, \{\mathbf{y}[\tau]\}_{\tau=0}^{P-1}$

Output: $\{\tilde{\mathbf{a}}_n[t]\}_{n=1}^N$

Initialization: $\tilde{\mathbf{a}}_n[P] = \mathbf{0}, n = 1, \dots, N, \Phi[P-1] = \sigma^2 \mathbf{I}$
 $\mathbf{r}_n[t] = \mathbf{0}, n = 1, \dots, N$

```

1: for  $t = P, P+1, \dots$  do
2:   Receive data vector  $\mathbf{y}[t]$ 
3:   Form  $\mathbf{g}[t]$  via (4)
4:    $\Phi[t] = \gamma \Phi[t-1] + \mu \mathbf{g}[t] \mathbf{g}^\top[t]$ 
5:   for  $n = 1, \dots, N$  do
6:      $\mathbf{r}_n[t] = \gamma \mathbf{r}_n[t-1] + \mu y_n[t] \mathbf{g}[t]$ 
7:      $\tilde{\mathbf{v}}_n[t] = \Phi[t] \tilde{\mathbf{a}}_n[t] - \mathbf{r}_n[t]$ 
8:     for  $n' = 1, 2, \dots, N$  do
9:        $\tilde{\mathbf{a}}_{n,n'}^f[t] = \tilde{\mathbf{a}}_{n,n'}[t] - \alpha_t \tilde{\mathbf{v}}_{n,n'}[t]$ 
10:      Compute  $\tilde{\mathbf{a}}_{n,n'}[t+1]$  via (24)
11:    end for
12:  end for
13: end for

```

To complement the arguments presented at the beginning of this section to support the decision of setting $f_t(\mathbf{a}_n) = \tilde{\ell}_t^{(n)}(\mathbf{a}_n)$, which laid the grounds to develop TIRSO, the rest of this section formally establishes that the batch problems that TISO and TIRSO implicitly solve become asymptotically equivalent as $T \rightarrow \infty$. To this end, let $\mathbf{a}_n^*[T]$ denote the hindsight solution for TISO, which is given by

$$\mathbf{a}_n^*[T] = \arg \min_{\mathbf{a}_n} C_T(\mathbf{a}_n), \quad (25)$$

where

$$C_T(\mathbf{a}_n) \triangleq \frac{1}{T-P} \sum_{t=P}^{T-1} \left[\tilde{\ell}_t^{(n)}(\mathbf{a}_n) + \lambda \sum_{n'=1, n' \neq n}^N \|\mathbf{a}_{n,n'}\|_2 \right]. \quad (26)$$

Observe that (26) is identical to the objective in the batch criterion (5). Likewise, let $\tilde{\mathbf{a}}_n^*[T]$ denote the hindsight solution of TIRSO, which is given by

$$\tilde{\mathbf{a}}_n^*[T] = \arg \min_{\mathbf{a}_n} \tilde{C}_T(\mathbf{a}_n), \quad (27)$$

with

$$\tilde{C}_T(\mathbf{a}_n) \triangleq \frac{1}{T-P} \sum_{t=P}^{T-1} \left[\tilde{\ell}_t^{(n)}(\mathbf{a}_n) + \lambda \sum_{n'=1, n' \neq n}^N \|\mathbf{a}_{n,n'}\|_2 \right]. \quad (28)$$

In this case, (28) no longer coincides with the objective in (5). Therefore, one could claim that the TIRSO algorithm is not pursuing the estimates that minimize the batch criterion (5). This idea is dispelled next by establishing the asymptotic equivalence between minimizing $\tilde{C}_T(\mathbf{a}_n)$ and minimizing $C_T(\mathbf{a}_n)$, since the latter is identical to (5).

Theorem 1. Assume that there exists $B_y \in \mathbb{R}$ such that $|y_n[t]|^2 \leq B_y \forall n, t$. Then:

- 1) It holds for all \mathbf{a}_n that $\lim_{T \rightarrow \infty} |C_T(\mathbf{a}_n) - \tilde{C}_T(\mathbf{a}_n)| = 0$.
- 2) It holds that $\lim_{T \rightarrow \infty} \left| \inf_{\mathbf{a}_n} C_T(\mathbf{a}_n) - \inf_{\mathbf{a}_n} \tilde{C}_T(\mathbf{a}_n) \right| = 0$.
- 3) If, additionally, there exists T_m such that

$$\frac{1}{T_m - P} \sum_{\tau=P}^{T_m} \mathbf{g}[\tau] \mathbf{g}^\top[\tau],$$

is positive definite, then $\lim_{T \rightarrow \infty} \|\mathbf{a}_n^*[T] - \tilde{\mathbf{a}}_n^*[T]\|_2 = 0$.

Proof: See the Appendix. ■

Theorem 1 essentially establishes not only that the TISO and TIRSO hindsight objectives are asymptotically the same but also that their minima and minimizers asymptotically coincide. Since the TISO hindsight objective equals the batch objective (5), it follows that the TIRSO hindsight objective asymptotically approaches the batch objective (5). This observation is very important since the regret analysis from Sec. IV will establish that the TISO and TIRSO estimates asymptotically match their hindsight counterparts. Note that the hypothesis of Theorem 1 entails no loss of generality in real-world applications, where data are bounded and therefore B_y must necessarily exist. Additionally, the hypothesis of part 3 also entails no loss of generality. To see this, note that if it does not hold, then part of the data is redundant and a non-redundant equivalent data set can be obtained upon applying a linear transformation to the given data set.

IV. PERFORMANCE ANALYSIS

This section characterizes the performance of TISO and TIRSO analytically. Specifically, it is shown that the sequences of estimates produced by these algorithms result in a sublinear regret, which is the basic objective in online optimization; see Sec. II-C. Broadly speaking, this property means that, on average and asymptotically, the online estimates perform as well as their hindsight counterparts.

Recall that h_t in the regret metric (7) is given by $h_t(\mathbf{a}) = f_t(\mathbf{a}) + \Omega(\mathbf{a})$. For TISO, f_t and Ω are given by (13) whereas, for TIRSO, f_t and Ω are respectively given by (21) and (13b).

The next result establishes sublinear regret for TISO.

Theorem 2. *Let $\{\mathbf{a}_n[t]\}_{t=P+1}^T$ be the sequence generated by TISO (Procedure 1) with constant step size $\alpha_t = \alpha = \mathcal{O}(1/\sqrt{T})$. If there exists $B_y \in \mathbb{R}$ such that $|y_n[t]|_2^2 \leq B_y, \forall t, n$, then*

$$R(T) = \mathcal{O}\left(PNB_y \|\mathbf{a}_n^*[T]\|_2^2 \sqrt{T}\right). \quad (29)$$

Proof: The first step is to verify that the hypotheses of [36, Corollary 5] are satisfied. In particular, $\rho > 0$ must be found such that $\|\nabla \ell_t^{(n)}(\mathbf{a}_n)\|_2^2 \leq \rho \ell_t^{(n)}(\mathbf{a}_n), \forall t, n$. To this end, note from (16) that

$$\begin{aligned} \|\nabla \ell_t^{(n)}(\mathbf{a}_n)\|_2^2 &= \|\mathbf{g}[t] (\mathbf{g}^\top[t] \mathbf{a}_n - y_n[t])\|_2^2 \\ &= \|\mathbf{g}[t]\|_2^2 \cdot |y_n[t] - \mathbf{g}^\top[t] \mathbf{a}_n|^2. \end{aligned} \quad (30)$$

On the other hand, the hypothesis $|y_n[t]|^2 \leq B_y \forall n, t$ implies that $\|\mathbf{y}[t]\|_2^2 \leq NB_y$ and, therefore,

$$\|\mathbf{g}[t]\|_2^2 = \sum_{\tau=t-P}^{t-1} \|\mathbf{y}[\tau]\|_2^2 \leq P \max_{t-P \leq \tau \leq t-1} \|\mathbf{y}[\tau]\|_2^2 \leq PNB_y. \quad (31)$$

Combining (30) and (31) yields

$$\|\nabla \ell_t^{(n)}(\mathbf{a}_n)\|_2^2 \leq PNB_y |y_n[t] - \mathbf{g}^\top[t] \mathbf{a}_n|^2. \quad (32)$$

Thus, to satisfy

$$\|\nabla \ell_t^{(n)}(\mathbf{a}_n)\|_2^2 \leq \rho \ell_t^{(n)}(\mathbf{a}_n) = \rho \frac{1}{2} (y_n[t] - \mathbf{g}^\top[t] \mathbf{a}_n)^2,$$

it suffices to set $\rho = 2PNB_y$. Using this bound and noting that the strong-convexity parameter of ψ (see (12)) adopted in TISO is 1, one can apply [36, Corollary 5] to obtain

$$\begin{aligned} R(T) &= \mathcal{O}\left(\frac{1}{2} \rho \sqrt{T-P} \|\mathbf{a}_n^*[T] - \mathbf{a}_n[P]\|_2^2\right) \\ &= \mathcal{O}\left(\frac{1}{2} \rho \sqrt{T} \|\mathbf{a}_n^*[T]\|_2^2\right) \\ &= \mathcal{O}\left(PNB_y \sqrt{T} \|\mathbf{a}_n^*[T]\|_2^2\right). \end{aligned} \quad \blacksquare$$

Clearly, the hypothesis of bounded $y_n[t]$ does not entail loss of generality in real-world applications. However, it can be seen that the regret order is linear in B_y , which is natural since the regret is expected to be greater whenever data are allowed to take values in a wider range. Similar observations apply to the rest of parameters involved in (29). Regarding the hypothesis $\alpha_t = \alpha = \mathcal{O}(1/\sqrt{T})$, one may wonder why a constant step size may evolve as $\mathcal{O}(1/\sqrt{T})$. This is indeed a common practice in online optimization (see e.g. [36]) and can be interpreted in terms of a sequence of algorithms that comprises one copy of TISO per value of T . Each algorithm in this sequence potentially has a different step size, but the same step size is used for all t by each algorithm. The rest of this section presents the regret analysis for TIRSO.

Theorem 3. *Let $\{\mathbf{a}_n[t]\}$ be the sequence generated by TIRSO (Procedure 2) with constant step size $\alpha_t = \alpha = \mathcal{O}(1/\sqrt{T})$. If $|y_n[t]|_2^2 \leq B_y, \forall t, n$, then*

$$R(T) = \mathcal{O}\left(\left[\sup_t \lambda_{\max}(\Phi[t])\right] \|\tilde{\mathbf{a}}_n^*[T]\|_2^2 \sqrt{T}\right). \quad (33)$$

Proof: The first step is to verify that the hypotheses of [36, Corollary 5] hold. To this end, one must find $\tilde{\rho} > 0$ such that

$$\|\nabla \tilde{\ell}_t^{(n)}(\mathbf{a}_n)\|_2^2 \leq \tilde{\rho} \tilde{\ell}_t^{(n)}(\mathbf{a}_n), \quad \forall t, n, \quad (34)$$

holds for all \mathbf{a}_n . From (22) and $\nabla \tilde{\ell}_t^{(n)}(\mathbf{a}_n) = \Phi[t] \mathbf{a}_n - \mathbf{r}_n[t]$, it follows that (34) is equivalent to

$$\begin{aligned} \|\Phi[t] \mathbf{a}_n - \mathbf{r}_n[t]\|_2^2 &\leq \tilde{\rho} \left(\frac{1}{2} \mathbf{a}_n^\top \Phi[t] \mathbf{a}_n - \mathbf{r}_n^\top[t] \mathbf{a}_n \right. \\ &\quad \left. + \frac{1}{2} \sum_{\tau=P}^t \mu \gamma^{t-\tau} y_n^2[\tau] \right), \quad \forall t, n. \end{aligned} \quad (35)$$

By expanding the left-hand side of (35), rearranging terms, and introducing $Z_t(\mathbf{a}_n)$ as

$$\begin{aligned} Z_t(\mathbf{a}_n) &\triangleq \mathbf{a}_n^\top \left(\frac{\tilde{\rho}}{2} \Phi[t] - \Phi^\top[t] \Phi[t] \right) \mathbf{a}_n + (2\mathbf{r}_n^\top[t] \Phi[t] \\ &\quad - \tilde{\rho} \mathbf{r}_n^\top[t]) \mathbf{a}_n + \frac{\tilde{\rho} \mu}{2} \sum_{\tau=P}^t \gamma^{t-\tau} y_n^2[\tau] - \mathbf{r}_n^\top[t] \mathbf{r}_n[t], \end{aligned} \quad (36)$$

the condition in (34) is equivalent to $Z_t(\mathbf{a}_n) \geq 0$. So the goal becomes finding $\tilde{\rho}$ such that $Z_t(\mathbf{a}_n) \geq 0$ for all \mathbf{a}_n and t . For this condition to hold, it is necessary that (a) $\inf_{\mathbf{a}_n} Z_t(\mathbf{a}_n)$ is

finite for all t , and (b) $\inf_{\mathbf{a}_n} Z_t(\mathbf{a}_n) \geq 0$ for all t . It can be seen [44, Appendix A.5] that condition (a) holds iff (a1) the Hessian matrix $\mathbf{H}Z_t(\mathbf{a}_n) = \tilde{\rho}\Phi[t] - 2\Phi^\top[t]\Phi[t]$ is positive semidefinite, and (a2) $2\Phi[t]\mathbf{r}_n[t] - \tilde{\rho}\mathbf{r}_n[t] \in \mathcal{R}(\mathbf{H}Z_t(\mathbf{a}_n))$, where $\mathcal{R}(\mathbf{A})$ denotes the span of the columns of a matrix \mathbf{A} . The first step is to find $\tilde{\rho}$ such that (a1) holds. To this end, consider the eigenvalue decomposition of $\Phi[t] = \mathbf{U}\Lambda\mathbf{U}^\top$, where the index t is omitted to simplify notation. Therefore,

$$\mathbf{H}Z_t(\mathbf{a}_n) = \mathbf{U}(\tilde{\rho}\Lambda - 2\Lambda^2)\mathbf{U}^\top. \quad (37)$$

Let $\lambda_{\max}(\Phi[t])$ denote the maximum eigenvalue of $\Phi[t]$. It follows from (37) that $\mathbf{H}Z_t(\mathbf{a}_n)$ is positive semidefinite if

$$\tilde{\rho} \geq 2\lambda_{\max}(\Phi[t]). \quad (38)$$

It remains to be shown that there exists $\tilde{\rho} > 0$ such that (38), (a2), and (b) simultaneously hold. To this end, focus first on (a2), which can be rewritten as

$$\begin{aligned} 2\Phi[t]\mathbf{r}_n[t] - \tilde{\rho}\mathbf{r}_n[t] &\in \mathcal{R}(\tilde{\rho}\Phi[t] - 2\Phi^\top[t]\Phi[t]) \\ &= \mathcal{R}(\Phi[t](\tilde{\rho}\mathbf{I} - 2\Phi[t])). \end{aligned} \quad (39)$$

Clearly, if $\tilde{\rho} > 2\lambda_{\max}(\Phi[t])$, then $\tilde{\rho}\mathbf{I} - 2\Phi[t]$ is invertible and, hence, $\mathcal{R}(\Phi[t](\tilde{\rho}\mathbf{I} - 2\Phi[t])) = \mathcal{R}(\Phi[t])$ [45, Ch. 4]. Thus, (39) holds if $2\Phi[t]\mathbf{r}_n[t] \in \mathcal{R}(\Phi[t])$ and $\tilde{\rho}\mathbf{r}_n[t] \in \mathcal{R}(\Phi[t])$. The former condition is trivial. To verify the latter, define

$$\mathbf{y}_n \triangleq [y_n[P], \dots, y_n[t]]^\top \in \mathbb{R}^{t-P+1 \times 1}, \quad (40a)$$

$$\mathbf{G} \triangleq [\mathbf{g}[P], \dots, \mathbf{g}[t]] \in \mathbb{R}^{N \times t-P+1}, \quad (40b)$$

$$\Gamma \triangleq \text{diag}(\mu[\gamma^{t-P}, \dots, \gamma^0]) \in \mathbb{R}^{t-P+1 \times t-P+1}, \quad (40c)$$

and $\mathbf{B} \triangleq \mathbf{G}\Gamma^{1/2}$; note that $\Phi[t] = \mathbf{G}\Gamma\mathbf{G}^\top = \mathbf{B}\mathbf{B}^\top$. It follows that $\mathbf{r}_n[t] = \mathbf{G}\Gamma\mathbf{y}_n = \mathbf{B}\Gamma^{1/2}\mathbf{y}_n \in \mathcal{R}(\mathbf{B}) = \mathcal{R}(\mathbf{B}\mathbf{B}^\top) = \mathcal{R}(\Phi[t])$. Therefore, $\tilde{\rho}\mathbf{r}_n[t] \in \mathcal{R}(\Phi[t])$ holds and, consequently, (a2) holds whenever $\tilde{\rho} > 2\lambda_{\max}(\Phi[t])$.

So far, this proof has established that, if $\tilde{\rho} > 2\lambda_{\max}(\Phi[t])$, then both (a1) and (a2) hold. The next step is to show that (b) also holds when $\tilde{\rho} > 2\lambda_{\max}(\Phi[t])$. To this end, set the gradient of $Z_t(\mathbf{a}_n)$ equal to zero and use $\tilde{\rho} > 2\lambda_{\max}(\Phi[t])$ to obtain $\Phi^\dagger[t]\mathbf{r}_n[t] \in \arg \min_{\mathbf{a}_n} Z_t(\mathbf{a}_n)$, where the symbol \dagger denotes pseudo-inverse. From this expression and (36), it follows that

$$\begin{aligned} \inf_{\mathbf{a}_n} Z_t(\mathbf{a}_n) &= Z_t(\Phi^\dagger[t]\mathbf{r}_n[t]) \\ &= \mathbf{r}_n^\top[t]\Phi^\dagger[t]\left(\frac{\tilde{\rho}}{2}\Phi[t] - \Phi^\top[t]\Phi[t]\right)\Phi^\dagger[t]\mathbf{r}_n[t] + (2\mathbf{r}_n^\top[t]\Phi[t] \\ &\quad - \tilde{\rho}\mathbf{r}_n^\top[t])\Phi^\dagger[t]\mathbf{r}_n[t] + \frac{\tilde{\rho}\mu}{2}\sum_{\tau=P}^t \gamma^{t-\tau}y_n^2[t] - \mathbf{r}_n^\top[t]\mathbf{r}_n[t]. \end{aligned}$$

Applying the properties of the pseudoinverse and simplifying results in

$$\inf_{\mathbf{a}_n} Z_t(\mathbf{a}_n) = \frac{\tilde{\rho}\mu}{2}\sum_{\tau=P}^t \gamma^{t-\tau}y_n^2[t] - \frac{\tilde{\rho}}{2}\mathbf{r}_n^\top[t]\Phi^\dagger[t]\mathbf{r}_n[t]. \quad (41)$$

From this expression, note that the condition $\inf_{\mathbf{a}_n} Z_t(\mathbf{a}_n) \geq 0$ is equivalent to

$$\mathbf{y}_n^\top\Gamma\mathbf{y}_n \geq \mathbf{y}_n^\top\Gamma\mathbf{G}^\top(\mathbf{G}\Gamma\mathbf{G}^\top)^\dagger\mathbf{G}\Gamma\mathbf{y}_n, \quad (42)$$

and, upon defining $\tilde{\mathbf{y}}_n \triangleq \Gamma^{1/2}\mathbf{y}_n$,

$$\tilde{\mathbf{y}}_n^\top\tilde{\mathbf{y}}_n \geq \tilde{\mathbf{y}}_n^\top\Gamma^{1/2}\mathbf{G}^\top(\mathbf{G}\Gamma\mathbf{G}^\top)^\dagger\mathbf{G}\Gamma^{1/2}\tilde{\mathbf{y}}_n. \quad (43)$$

This inequality trivially holds when $\tilde{\mathbf{y}}_n = \mathbf{0}$. Thus, assume without loss of generality that $\tilde{\mathbf{y}}_n \neq \mathbf{0}$. By setting $\mathbf{A} \triangleq \Gamma^{1/2}\mathbf{G}^\top(\mathbf{G}\Gamma\mathbf{G}^\top)^\dagger$, one obtains $\mathbf{A}\mathbf{B} = \Gamma^{1/2}\mathbf{G}^\top(\mathbf{G}\Gamma\mathbf{G}^\top)^\dagger\mathbf{G}\Gamma^{1/2}$ and $\mathbf{B}\mathbf{A} = \Phi[t]\Phi^\dagger[t]$.

Since the nonzero eigenvalues of $\mathbf{A}\mathbf{B}$ and $\mathbf{B}\mathbf{A}$ are the same [46, Sec. 3.2.11] and the maximum eigenvalue of $\mathbf{B}\mathbf{A}$ is 1, then the maximum eigenvalue of $\mathbf{A}\mathbf{B}$ is also 1. Therefore

$$\frac{\tilde{\mathbf{y}}_n^\top\mathbf{A}\mathbf{B}\tilde{\mathbf{y}}_n}{\tilde{\mathbf{y}}_n^\top\tilde{\mathbf{y}}_n} = \frac{\tilde{\mathbf{y}}_n^\top\Gamma^{1/2}\mathbf{G}^\top(\mathbf{G}\Gamma\mathbf{G}^\top)^\dagger\mathbf{G}\Gamma^{1/2}\tilde{\mathbf{y}}_n}{\tilde{\mathbf{y}}_n^\top\tilde{\mathbf{y}}_n} \leq 1, \quad (44)$$

and, hence, (43) holds. To sum up, conditions (a) and (b) hold if $\tilde{\rho} > 2\lambda_{\max}(\Phi[t])$. In other words, (34) holds for any choice of $\tilde{\rho}$ such that $\tilde{\rho} > 2\lambda_{\max}(\Phi[t])$ for all t .

To obtain the desired regret expression, set $\tilde{\rho} = \sup_t \lambda_{\max}(\Phi[t]) + \epsilon$ with $\epsilon > 0$ an arbitrary constant, and invoke [36, Corollary 5] to conclude that

$$R(T) = \mathcal{O}\left(\tilde{\rho}\|\tilde{\mathbf{a}}_n^*[T]\|_2^2\sqrt{T}\right). \quad \blacksquare$$

Theorem 3 has the same form as Theorem 2 with the exception of (33), where the constants multiplying \sqrt{T} differ from those in (29). However, it is easy to show that TIRSO will also satisfy (29). To this end, use (23), (31), and Cauchy-Schwartz inequality to obtain (recall that $\mu = 1 - \gamma$)

$$\lambda_{\max}(\Phi[t]) = \sup_{\mathbf{z}: \|\mathbf{z}\|_2=1} \mathbf{z}^\top\Phi[t]\mathbf{z} \quad (45a)$$

$$= \sup_{\mathbf{z}: \|\mathbf{z}\|_2=1} \mu \sum_{\tau=P}^t \gamma^{t-\tau} \mathbf{z}^\top \mathbf{g}[\tau] \mathbf{g}^\top[\tau] \mathbf{z} \quad (45b)$$

$$\leq \sup_{\mathbf{z}: \|\mathbf{z}\|_2=1} \mu \sum_{\tau=P}^t \gamma^{t-\tau} \|\mathbf{z}\|_2^2 \|\mathbf{g}[\tau]\|_2^2 \quad (45c)$$

$$= \mu \sum_{\tau=P}^t \gamma^{t-\tau} \|\mathbf{g}[\tau]\|_2^2 \quad (45d)$$

$$\leq \mu \sum_{\tau=P}^t \gamma^{t-\tau} PNB_y \leq PNB_y. \quad (45e)$$

It follows that the right hand side of (33) can be replaced with the right hand side of (29) and the resulting expression will still hold.

To sum up, both TISO and TIRSO behave asymptotically in the same fashion and provide, on average, the same performance as the hindsight solution of TISO, which coincides with the batch solution from (5). The difference between TISO and TIRSO is, therefore, in the non-asymptotic regime, where TIRSO can track changes in the estimated graph more swiftly than TISO. This is at the expense of a slight increase in the number of arithmetic operations and required memory. Note, however, that TIRSO offers an additional degree of freedom through the selection of the forgetting factor γ . This enables the user to select the desired point in the tradeoff between adaptability to changes and robustness to noise.

V. NUMERICAL RESULTS AND ANALYSIS

Simulation tests for the proposed algorithms are performed on both synthetic data and real data. The proposed algorithms are evaluated based on the performance metrics described next. For synthetic data experiments, the normalized mean square deviation (NMSD) measures the difference between the true

coefficients of the VAR model generating the data and the estimated coefficients. It is defined as

$$\text{NMSD}[t] \triangleq \frac{\mathbb{E}[\sum_{n=1}^N \|\hat{\mathbf{a}}_n[t] - \mathbf{a}_n[t]\|_2^2]}{\mathbb{E}[\sum_{n=1}^N \|\mathbf{a}_n[t]\|_2^2]}. \quad (46)$$

The ability to detect edges of the true VAR-causality graph is assessed using the probability of miss detection

$$P_{\text{MD}}[t] \triangleq \frac{\sum_{n,n'=1}^N \mathbb{E}[\mathbb{1}\{\|\hat{\mathbf{a}}_{n,n'}[t]\|_2 < \delta\} \mathbb{1}\{\|\mathbf{a}_{n,n'}\|_2 \neq 0\}]}{\sum_{n=1}^N \sum_{n'=1}^N \mathbb{E}[\mathbb{1}\{\|\mathbf{a}_{n,n'}\|_2 \neq 0\}]}, \quad (47)$$

for a given threshold δ , which is the probability of not identifying an edge that actually exists, and the probability of false alarm

$$P_{\text{FA}}[t] \triangleq \frac{\sum_{n,n'=1}^N \mathbb{E}[\mathbb{1}\{\|\hat{\mathbf{a}}_{n,n'}[t]\|_2 \geq \delta\} \mathbb{1}\{\|\mathbf{a}_{n,n'}\|_2 = 0\}]}{\sum_{n=1}^N \sum_{n'=1}^N \mathbb{E}[\mathbb{1}\{\|\mathbf{a}_{n,n'}\|_2 = 0\}]}, \quad (48)$$

which is the probability of detecting an edge that does not exist. Another relevant metric is the edge identification error rate, which measures how many edges are misidentified relative to the number of possible edges [47]:

$$\text{EIER}[t] = \frac{1}{N(N-1)} \sum_{n=0}^{N-1} \sum_{n'=0, n' \neq n}^{N-1} \mathbb{E}[\mathbb{1}\{\|\hat{\mathbf{a}}_{n,n'}[t]\|_2 \geq \delta\} - \mathbb{1}\{\|\mathbf{a}_{n,n'}\|_2 \neq 0\}]. \quad (49)$$

Note that self-loops are excluded in this metric. To quantify the forecasting performance, define recursively the h -step ahead predictor given $\{\mathbf{y}[\tau]\}_{\tau \leq t}$ as follows:

$$\hat{\mathbf{y}}[t+h|t] \triangleq \sum_{p=1}^P \hat{\mathbf{A}}_p[t] \hat{\mathbf{y}}[t+h-p|t], \quad (50)$$

where $\{\hat{\mathbf{A}}_p[t]\}_{p=1}^P$ are the estimated VAR coefficients at time t and $\hat{\mathbf{y}}[t+j|t] = \mathbf{y}[t+j]$ for $j \leq 0$. The h -step normalized mean square error is given by

$$\text{NMSE}_h[t] = \frac{\mathbb{E}[\|\mathbf{y}[t+h] - \hat{\mathbf{y}}[t+h|t]\|_2^2]}{\mathbb{E}[\|\mathbf{y}[t+h]\|_2^2]}. \quad (51)$$

The values of all parameters involved in the experiments are listed in the captions and legends of the figures.

A. Synthetic Data Tests

Throughout this section, unless otherwise stated, the expectations in equations (46) to (51) are taken with respect to realizations of the graph, VAR parameters, and innovation process $\mathbf{u}[t]$. Likewise, the step size is set to $\alpha_t = 1/(4\lambda_{\max}(\Phi[t]))$.

1) *Stationary VAR Processes*: An Erdős-Rényi random graph is generated with edge probability p_e and self-loop probability 1. This graph determines which entries of the matrices $\{\mathbf{A}_p\}_{p=0}^P$ are zero. The rest of entries are drawn i.i.d. from a standard normal distribution. Matrices $\{\mathbf{A}_p\}_{p=0}^P$ are scaled down afterwards by a constant that ensures that the VAR process is stable [22]. The innovation process samples are drawn independently as $\mathbf{u}[t] \sim \mathcal{N}(\mathbf{0}, \sigma^2 \mathbf{I}_{N \times N})$.

The first experiment analyzes the performance of TISO and TIRSO in a stationary setting. Figs. 1(a) and 1(b) depict the NMSD and NMSE₁ for three different values of λ . As

a benchmark, Fig. 1(b) includes the NMSE₁ of the *genie-aided predictor*, obtained from (50) after replacing $\hat{\mathbf{A}}_p$ with \mathbf{A}_p . It is observed that $\lambda = 10^{-6}$ yields a better NMSD and NMSE₁ than lower and higher values of λ . This corroborates the importance of promoting sparse solutions, as done in TISO and TIRSO, and of adjusting λ to the appropriate level of sparsity in the model parameters. Furthermore, as expected, TIRSO generally converges faster than TISO.

Fig. 1(c) shows the receiver operating characteristic (ROC) curve, composed of pairs $(P_{\text{FA}}, P_{\text{MD}})$ for different values of the threshold δ . The values of these pairs are obtained by respectively averaging $P_{\text{FA}}[t]$ and $P_{\text{MD}}[t]$ over time in the interval $[T_1, T_2]$. Remarkably, both TISO and TIRSO can simultaneously attain P_{FA} and P_{MD} below 10 %. This ability to satisfactorily detect edges is further investigated in Figs. 1(d-f), where δ is set so that $P_{\text{FA}}[t]$ and $P_{\text{MD}}[t]$ have the same average in the time interval $[T_1, T_2]$.

Fig. 2 compares the true (left) and recovered (right) graphs via TIRSO and TISO by thresholding the average of the estimated VAR coefficients across the intervals $[k/(3T), (k+1)/(3T)]$, $k = 0, 1, 2$. The threshold δ is selected such that the algorithm detects $p_e(N^2 - N)$ edges. Note that this is not a Monte Carlo experiment. It is observed that both TIRSO and TISO can identify the true graph quite accurately and approximate the true VAR coefficients soon afterwards.

2) *Non-stationary VAR Processes*: The next experiment analyzes TISO and TIRSO when $\mathbf{y}[t]$ is a (non-stationary) smooth-transition VAR process [48, Ch. 18]:

$$\mathbf{y}[t] = \sum_{p=1}^P (\mathbf{A}_p + s_f[t](\mathbf{B}_p - \mathbf{A}_p)) \mathbf{y}[t-p] + \mathbf{u}[t]. \quad (52)$$

The signal $s_f[t]$ determines the transition profile from a VAR model with parameters $\{\mathbf{A}_p\}_p$ to a VAR model with parameters $\{\mathbf{B}_p\}_p$. In this experiment, $s_f[t] = 1 - \exp(-\kappa((t - T_B)_+)^2)$, where $\kappa > 0$ controls the transition speed and T_B denotes transition starting instant. Over an Erdős-Rényi random graph, $\{\mathbf{A}_p\}$ and $\{\mathbf{B}_p\}$ are generated independently as in Sec. V-A1. It is easy to show that the coefficients $\mathbf{A}_p + s_f[t](\mathbf{B}_p - \mathbf{A}_p)$ yield a *stable* VAR processes for all t .

Figs. 3(a) and 3(b) illustrate the influence of the forgetting factor γ , of critical importance in non-stationary setups. TISO and TIRSO are seen to satisfactorily estimate and track the model coefficients. As intuition predicts, the lower γ is, the more rapidly TIRSO can adapt to changes, but after a sufficiently long time after the transition, a higher γ is preferred.

Finally, to demonstrate that TISO and TIRSO successfully leverage sparsity to track *time-varying* topologies, Fig. 4 illustrates that λ must be matched to the degree of sparsity in the true graph.

B. Real Data Tests

The real data used in the experiments of this paper are taken from Lundin's offshore oil and gas (O&G) platform Edvard-Grieg². Each node corresponds to a temperature, pressure, or oil-level sensor placed in one of the separators of a system that separates oil, gas, and water. A separator is essentially a decantation tank. The measured time series are physically

²<https://www.lundin-petroleum.com/operations/production/norway-edvard-grieg>

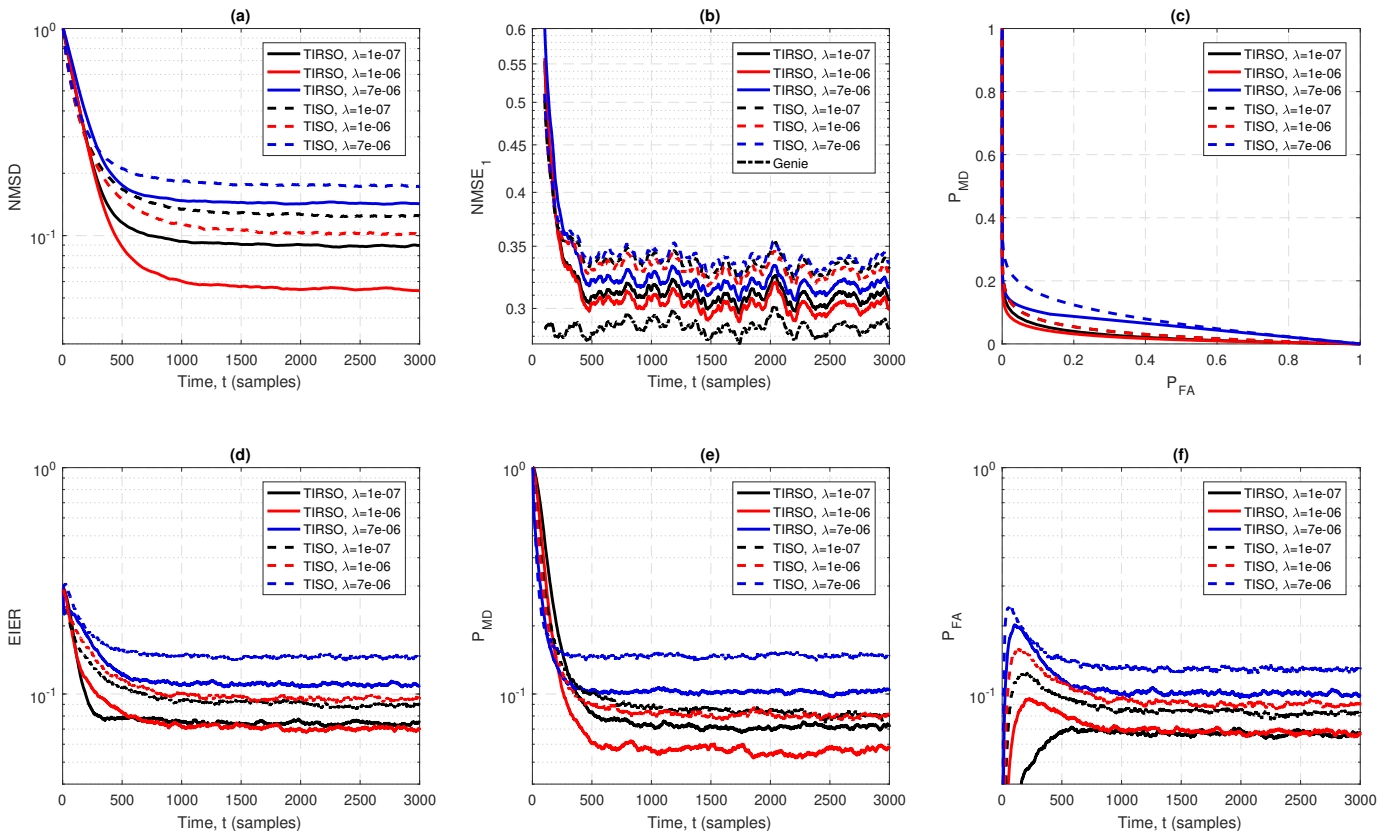


Fig. 1: Performance of TISO and TIRSO on stationary time series for different degrees of sparsity-promoting regularization ($N = 12$, $P = 2$, $p_e = 0.2$, $\sigma = 0.005$, $\gamma = 0.99$, $T = 3000$, $T_1 = 500$, $T_2 = 3000$, 300 Monte Carlo runs).

coupled due to the pipelines connecting the system parts and due to the control systems. Hence, causal relations among them are expected. Topology identification is motivated in this context to predict the future state of the system and to unveil dependencies that are cannot be detected by simple inspection. All time series are resampled to a common set of equally-spaced sampling instants using linear interpolation. Since the data were quantized and compressed using a lossy scheme, a significant amount of noise is expected. Each time series is normalized to have zero mean and unit sample standard deviation.

In this section, the step size is set to $\alpha_t = 1/(\lambda_{\max}(\Phi[t]))$ and the NMSE is defined as

$$\text{NMSE}_h = \frac{\sum_t \|\mathbf{y}[t+h] - \hat{\mathbf{y}}[t+h]\|_2^2}{\sum_t \|\mathbf{y}[t+h]\|_2^2}. \quad (53)$$

Fig. 5 shows the NMSE_h vs. the *prediction horizon* h for the time series in the data set. The temperature, pressure, and oil level time series are respectively denoted by T, P, and L and an identifying index. As expected, the prediction error increases with h . The normalized prediction error of the time series ranges between 10^{-4} and 1 mainly because of their different variability and predictability.

Fig. 6 presents the graph obtained by thresholding the result of averaging the estimated coefficients over three hours. The threshold is such as the number of edges is in the order of the number of nodes in the network. The self-loops are omitted in the figure for clarity. The color of the arrows corresponds

to the weight of the corresponding edge. It is observed that most of the observed edges are among variables in the same separator.

VI. CONCLUSIONS

This paper presented two online algorithms for identifying VAR-causality graphs. These algorithms accommodate data as received and refine their topology estimates accordingly. Using the framework of online optimization and pursuing a *composite* approach, each update provides a sparse topology. Theoretical analysis reveals that both algorithms are asymptotically equivalent and asymptotically attain the average performance of their batch counterparts. The proposed algorithms offer complementary benefits: whereas TISO is computationally simpler, TIRSO showcases improved convergence behaviour. Experiments with synthetic and real data validate the conclusions of the theoretical analysis. Future work includes explicitly modeling the variations in the VAR coefficients, possibly along the lines of [49]–[51].

REFERENCES

- [1] B. Zaman, L. M. López-Ramos, D. Romero, and B. Bekerull-Lozano, "Online topology estimation for vector autoregressive processes in data networks," in *Proc. IEEE Int. Workshop Comput. Advan. Multi-Sensor Adapt. Process.*, Curaçao, Dutch Antilles, Dec. 2017.
- [2] E. D. Kolaczyk, *Statistical Analysis of Network Data: Methods and Models*, Springer, New York, 2009.
- [3] E. Isufi, A. Loukas, N. Perraudin, and G. Leus, "Forecasting time series with varma recursions on graphs," *arXiv preprint arXiv:1810.08581*, 2018.

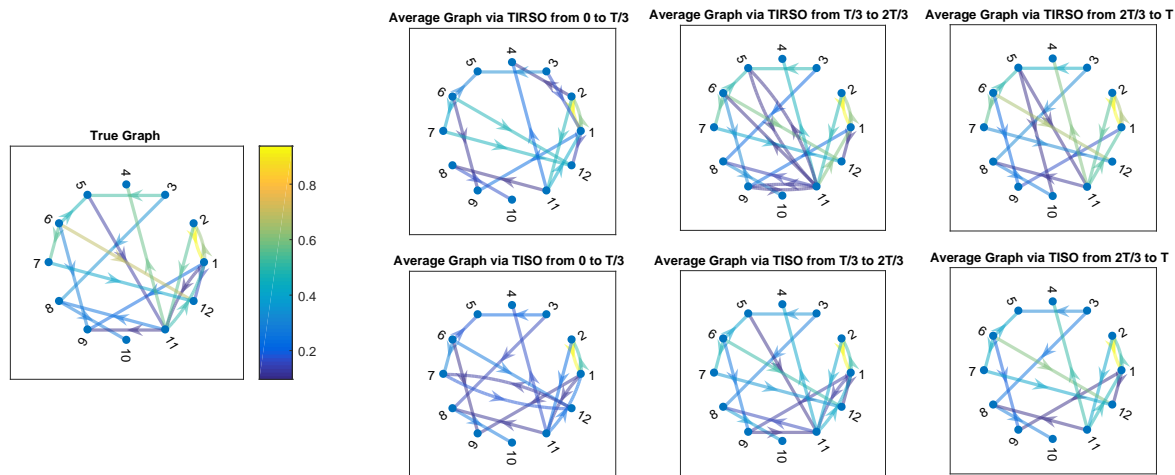


Fig. 2: True and recovered graphs ($N = 12$, $P = 2$, $p_e = 0.2$, $\sigma = 0.005$, $\gamma = 0.98$, $\lambda = 10^{-6}$, $T = 600$).

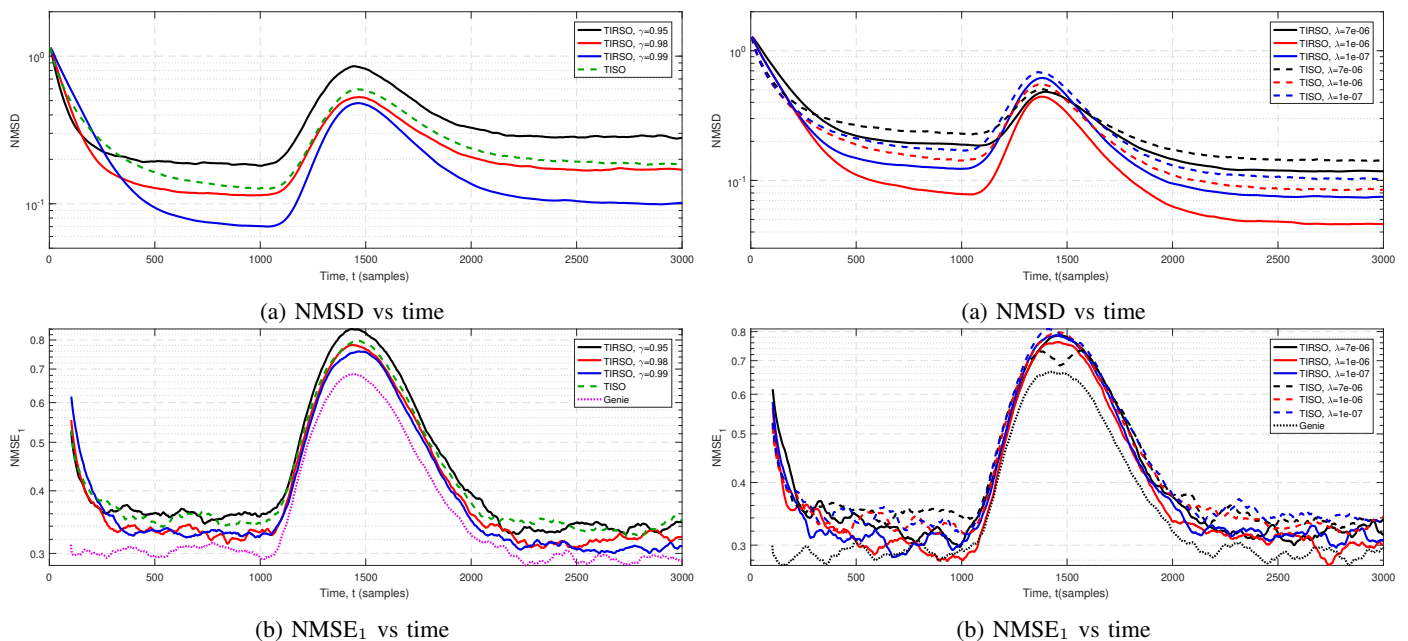


Fig. 3: Effect of the forgetting factor on the performance in a smooth-transition VAR model ($\kappa = 0.99$, $T_B = 1000$, $N = 12$, $P = 2$, $p_e = 0.2$, 300 Monte Carlo runs).

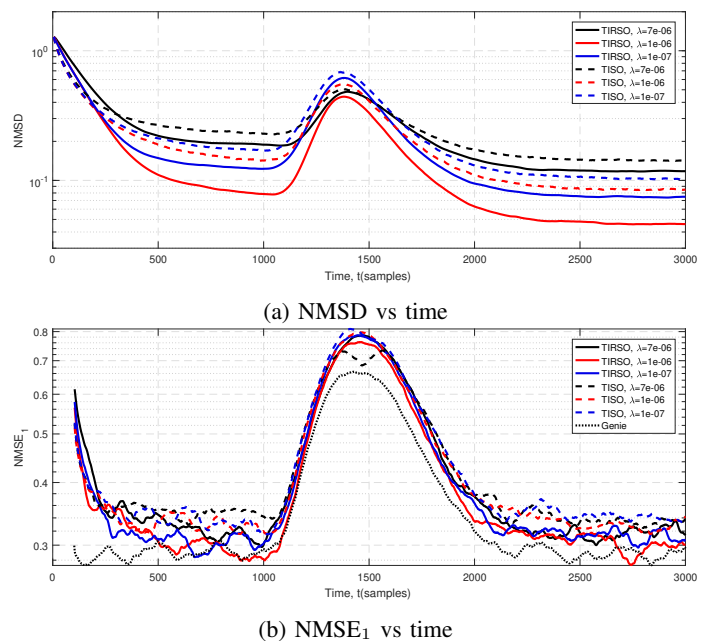


Fig. 4: Effect of the regularization parameter on the performance in a smooth-transition VAR model ($\kappa = 0.99$, $T_B = 1000$, $N = 12$, $T = 3000$, $P = 2$, $p_e = 0.2$, 200 Monte-Carlo runs).

- [4] P. Di Lorenzo, S. Barbarossa, P. Banelli, and S. Sardellitti, "Adaptive least mean squares estimation of graph signals," *IEEE Trans. Sig. Info. Process. Netw.*, vol. 2, no. 4, pp. 555–568, Dec. 2016.
- [5] C. Liu, S. Ghosal, Z. Jiang, and S. Sarkar, "An unsupervised spatiotemporal graphical modeling approach to anomaly detection in distributed CPS," in *ACM/IEEE Int. Conf. Cyber-Physical Syst.*, Apr. 2016, pp. 1–10.
- [6] Y. Shen, P. A. Traganitis, and G. B. Giannakis, "Nonlinear dimensionality reduction on graphs," in *Proc. IEEE Int. Workshop Comput. Advan. Multi-Sensor Adapt. Process.*, Curacao, Netherlands Antilles, Dec. 2017.
- [7] G. Mateos, S. Segarra, A. G. Marques, and A. Ribeiro, "Connecting the dots: Identifying network structure via graph signal processing," *arXiv preprint arXiv:1810.13066*, 2018.
- [8] D. Angelosante and G. B. Giannakis, "Sparse graphical modeling of piecewise-stationary time series," in *Proc. IEEE Int. Conf. Acoust., Speech, Sig. Process.*, Prague, Czech Republic, 2011, pp. 1960–1963.
- [9] J. Friedman, T. Hastie, and R. Tibshirani, "Sparse inverse covariance estimation with the graphical lasso," *Biostatistics*, vol. 9, no. 3, pp. 432–441, 2008.
- [10] S. L. Lauritzen, *Graphical Models*, vol. 17, Clarendon Press, 1996.
- [11] C. M. Bishop, *Pattern Recognition and Machine Learning*, Information Science and Statistics. Springer, 2006.
- [12] X. Dong, D. Thanou, P. Frossard, and P. Vandergheynst, "Learning Laplacian matrix in smooth graph signal representations," *IEEE Trans. Sig. Process.*, vol. 64, no. 23, pp. 6160–6173, Dec. 2016.
- [13] S. Segarra, A. G. Marques, G. Mateos, and A. Ribeiro, "Network topology inference from spectral templates," *IEEE Trans. Sig. Info. Process. Netw.*, vol. 3, no. 3, pp. 467–483, Sept 2017.
- [14] R. B. Kline, *Principles and Practice of Structural Equation Modeling*, Guilford Publications, 2015.
- [15] Y. Shen, B. Baingana, and G. B. Giannakis, "Tensor decompositions for identifying directed graph topologies and tracking dynamic networks," *IEEE Trans. Sig. Process.*, vol. 65, no. 14, pp. 3675–3687, Jul. 2017.
- [16] C. W. J. Granger, "Some recent development in a concept of causality," *J. Econometrics*, vol. 39, no. 1-2, pp. 199–211, Sep. 1988.
- [17] A. Zellner, "Causality and econometrics," in *Carnegie-Rochester*

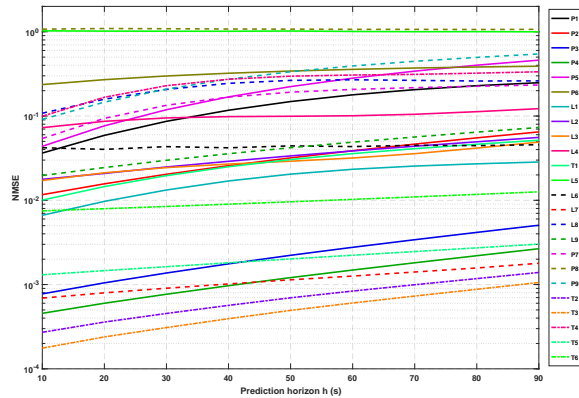


Fig. 5: Prediction NMSE vs. prediction horizon for individual variables of oil, gas, and water separation system. TIRSO is used with $P = 8$, $\gamma = 0.9$, $T = 4$ hours, sampling interval = 10 s. The regularization parameter λ is selected such that it minimizes the average NMSE.

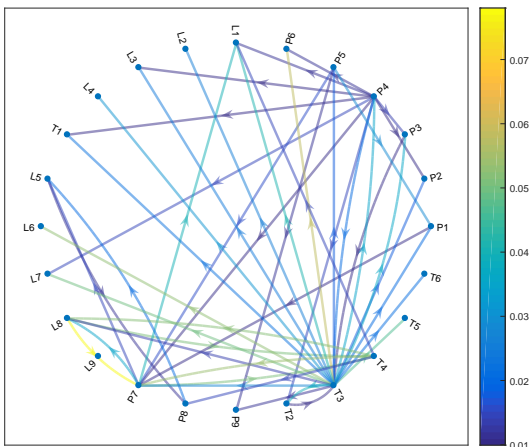


Fig. 6: The estimated topology of a subset of the variables. The sampling interval is set to 10 seconds. The topology is obtained via TIRSO with $\gamma = 0.9$, $T = 3$ hours, and $P = 8$. The regularization parameter λ is selected such that it minimizes the average NMSE.

Conference series on Public Policy. Elsevier, 1979, vol. 10, pp. 9–54.

[18] S. M. Kay, *Fundamentals of Statistical Signal Processing, Vol. I: Estimation Theory*, Prentice-Hall, 1993.

[19] R. Goebel, A. Roebroeck, D.S. Kim, and E. Formisano, “Investigating directed cortical interactions in time-resolved fmri data using vector autoregressive modeling and Granger causality mapping,” *Magnet. Reson. Imag.*, vol. 21, no. 10, pp. 1251–1261, 2018.

[20] S. Basu, A. Shojaie, and G. Michailidis, “Network Granger causality with inherent grouping structure,” *J. Mach. Learn. Res.*, vol. 16, no. 2, pp. 417–453, Mar. 2015.

[21] A. Tank, I. Covert, N. Foti, A. Shojaie, and E. Fox, “Neural Granger causality for nonlinear time series,” *arXiv preprint arXiv:1802.05842*, 2018.

[22] H. Lütkepohl, *New Introduction to Multiple Time Series Analysis*, Springer, 2005.

[23] J. L. Lions, *Optimal Control of Systems Governed by Partial Differential Equations*, vol. 170, Springer Berlin, 1971.

[24] H. Lütkepohl, M. Krätzig, and P. CB Phillips, *Applied Time Series Econometrics*, Cambridge University Press, 2004.

[25] A. Fujita, J. R. Sato, H. M. Garay-Malpartida, R. Yamaguchi, S. Miyano, M. C. Sogayar, and C. E. Ferreira, “Modeling gene expression regulatory networks with the sparse vector autoregressive model,” *BMC Syst. Bio.*, vol. 1, no. 1, pp. 39, 2007.

[26] P. A. Valdés-Sosa, J. M. Sánchez-Bornot, A. Lage-Castellanos, M. Vega-Hernández, J. Bosch-Bayard, L. Melie-García, and E. Canales-Rodríguez, “Estimating brain functional connectivity with sparse multivariate autoregression,” *Philosoph. Trans. Royal Soc. London B: Bio. Sci.*, vol. 360, no. 1457, pp. 969–981, 2005.

[27] F. R. Bach and M. I. Jordan, “Learning graphical models for stationary time series,” *IEEE Trans. Sig. Process.*, vol. 52, no. 8, pp. 2189–2199, Aug. 2004.

[28] J. Songsiri and L. Vandenberghe, “Topology selection in graphical models of autoregressive processes,” *J. Mach. Learn. Res.*, vol. 11, pp. 2671–2705, Oct. 2010.

[29] A. Bolstad, B. D. Van Veen, and R. Nowak, “Causal network inference via group sparse regularization,” *IEEE Trans. Sig. Process.*, vol. 59, no. 6, pp. 2628–2641, Jun. 2011.

[30] J. Songsiri, “Sparse autoregressive model estimation for learning Granger causality in time series,” in *Proc. IEEE Int. Conf. Acoust., Speech, Sig. Process.*, Vancouver, BC, Canada, May 2013, pp. 3198–3202.

[31] J. Mei and J. M. F. Moura, “Signal processing on graphs: Causal modeling of unstructured data,” *IEEE Trans. Sig. Process.*, vol. 65, no. 8, pp. 2077–2092, Apr. 2017.

[32] M. Kolar, L. Song, A. Ahmed, and E. P. Xing, “Estimating time-varying networks,” *Ann. Appl. Statist.*, pp. 94–123, 2010.

[33] J. Lee, G. Li, and J. D. Wilson, “Varying-coefficient models for dynamic networks,” *arXiv preprint arXiv:1702.03632*, 2017.

[34] D. Hallac, Youngsuk Park, S. Boyd, and J. Leskovec, “Network inference via the time-varying graphical lasso,” in *Proc. ACM SIGKDD Int. Conf. Knowled. Discov. Data Min.*, 2017, pp. 205–213.

[35] Y. Shen and G. B. Giannakis, “Online identification of directional graph topologies capturing dynamic and nonlinear dependencies,” in *IEEE Data Sci. Workshop*, 2018, pp. 195–199.

[36] J. Duchi, S. Shalev-Shwartz, Y. Singer, and A. Tewari, “Composite objective mirror descent,” in *Proc. of Annu. Conf. Computat. Learn. Theory*, 2010, pp. 14–26.

[37] M. Yuan and Y. Lin, “Model selection and estimation in regression with grouped variables,” *J. Royal Statist. Soc.: Series B (Statist. Method.)*, vol. 68, no. 1, pp. 49–67, 2006.

[38] S. Shalev-Shwartz, “Online learning and online convex optimization,” *Found. Trends Mach. Learn.*, vol. 4, no. 2, pp. 107–194, 2011.

[39] L. Xiao, “Dual averaging methods for regularized stochastic learning and online optimization,” *J. Mach. Learn. Res.*, vol. 11, pp. 2543–2596, 2010.

[40] A. T. Puig, A. Wiesel, G. Fleury, and A. O. Hero, “Multidimensional shrinkage-thresholding operator and group lasso penalties,” *IEEE Sig. Process. Lett.*, vol. 18, no. 6, pp. 363–366, Jun. 2011.

[41] E. M. Eksioğlu and A. K. Tanc, “RLS algorithm with convex regularization,” *IEEE Sig. Process. Lett.*, vol. 18, no. 8, pp. 470–473, Aug. 2011.

[42] H. Yang, Z. Xu, I. King, and M. R. Lyu, “Online learning for group lasso,” in *Proc. Int. Conf. Mach. Learn.*, Haifa, Israel, 2010.

[43] D. Angelosante, J. A. Bazerque, and G. B. Giannakis, “Online adaptive estimation of sparse signals: where RLS meets the ℓ_1 -norm,” *IEEE Trans. Sig. Process.*, vol. 58, no. 7, pp. 3436–3447, Jul. 2010.

[44] S. Boyd and L. Vandenberghe, *Convex Optimization*, Cambridge University Press, Cambridge, UK, 2004.

[45] Carl D Meyer, *Matrix Analysis and Applied Linear Algebra*, vol. 71, Siam, 2000.

[46] R. A. Horn and C. R. Johnson, *Matrix Analysis*, Cambridge University Press, Cambridge, UK, 1985.

[47] G. B. Giannakis, Y. Shen, and G. V. Karanikolas, “Topology identification and learning over graphs: Accounting for nonlinearities and dynamics,” *Proc. IEEE*, vol. 106, no. 5, pp. 787–807, May 2018.

[48] L. Kilian and H. Lütkepohl, *Structural Vector Autoregressive Analysis*, Cambridge University Press, 2017.

[49] Y. I. Abramovich, N. K. Spencer, and M. D. E. Turley, “Time-varying autoregressive (TVAR) adaptive order and spectrum estimation,” in *Proc. Asilomar Conf. Sig., Syst., Comput.*, Pacific Grove, CA, 2005.

[50] Y. I. Abramovich, N. K. Spencer, and M. D. E. Turley, “Order estimation and discrimination between stationary and time-varying (TVAR) autoregressive models,” *IEEE Trans. Sig. Process.*, vol. 55, no. 6, pp. 2861–2876, Jun. 2007.

[51] S. Lundbergh, T. Teräsvirta, and D. V. Dijk, "Time-varying smooth transition autoregressive models," *J. Bus. Econ. Stat.*, vol. 21, no. 1, pp. 104–121, Jan. 2003.

APPENDIX
PROOF OF THEOREM 1

The first step is to rewrite (28) to be able to obtain a simple expression for $C_T(\mathbf{a}_n) - \tilde{C}_T(\mathbf{a}_n)$. To this end, substitute (21) into (28) and exchange the order of the summations to obtain

$$\begin{aligned}\tilde{C}_T(\mathbf{a}_n) &= \frac{1}{T-P} \sum_{\tau=P}^{T-1} \left[\sum_{t=\tau}^{T-1} \gamma^{t-\tau} \mu \ell_\tau^{(n)}(\mathbf{a}_n) + \lambda \sum_{\substack{n'=1 \\ n' \neq n}}^N \|\mathbf{a}_{n,n'}\|_2 \right] \\ &= \frac{1}{T-P} \sum_{\tau=P}^{T-1} \theta_{\tau,T} \mu \ell_\tau^{(n)}(\mathbf{a}_n) + \lambda \sum_{n'=1, n' \neq n}^N \|\mathbf{a}_{n,n'}\|_2,\end{aligned}$$

where $\theta_{\tau,T} \triangleq \sum_{t=\tau}^{T-1} \gamma^{t-\tau}$. From the geometric series summation formula, which establishes that $\theta_{\tau,T} = (1 - \gamma^{T-\tau})/(1 - \gamma)$, and noting that $\mu = 1 - \gamma$, the above equation becomes

$$\tilde{C}_T(\mathbf{a}_n) = \frac{1}{T-P} \sum_{\tau=P}^{T-1} (1 - \gamma^{T-\tau}) \ell_\tau^{(n)}(\mathbf{a}_n) + \lambda \sum_{\substack{n'=1 \\ n' \neq n}}^N \|\mathbf{a}_{n,n'}\|_2.$$

From (26) and the equation above, the difference $d_T(\mathbf{a}_n) \triangleq C_T(\mathbf{a}_n) - \tilde{C}_T(\mathbf{a}_n)$ between the TISO and TIRSO hindsight objectives is given by:

$$d_T(\mathbf{a}_n) = \frac{1}{T-P} \sum_{\tau=P}^{T-1} \gamma^{T-\tau} \ell_\tau^{(n)}(\mathbf{a}_n). \quad (54)$$

To prove part 1, it suffices to show that $d_T(\mathbf{a}_n) \rightarrow 0$ as $T \rightarrow \infty$ for all \mathbf{a}_n . To this end, expand $\ell_t^{(n)}(\mathbf{a}_n)$

$$\ell_t^{(n)}(\mathbf{a}_n) = \frac{1}{2} (y_n^2[t] + \mathbf{a}_n^\top \mathbf{g}[t] \mathbf{g}^\top[t] \mathbf{a}_n - 2y_n[t] \mathbf{g}^\top[t] \mathbf{a}_n). \quad (55)$$

and apply Cauchy-Schwarz inequality to obtain

$$\ell_t^{(n)}(\mathbf{a}_n) \leq \frac{1}{2} [\|\mathbf{a}_n\| \cdot \|\mathbf{g}[t]\|]^2 + \frac{1}{2} B_y + \sqrt{B_y} \|\mathbf{g}[t]\|_2 \cdot \|\mathbf{a}_n\|_2. \quad (56)$$

On the other hand, the hypothesis $|y_n[t]|^2 \leq B_y \forall n, t$ implies that $\|\mathbf{y}[t]\|_2^2 \leq NB_y$, and hence

$$\|\mathbf{g}[t]\|_2^2 = \sum_{\tau=t-P}^{t-1} \|\mathbf{y}[\tau]\|_2^2 \leq P \max_{t-P \leq \tau \leq t-1} \|\mathbf{y}[\tau]\|_2^2 \leq PNB_y.$$

Substituting the upper bound of $\|\mathbf{g}[t]\|_2^2$ into (56) yields

$$\ell_t^{(n)}(\mathbf{a}_n) \leq \frac{1}{2} NP B_y \|\mathbf{a}_n\|_2^2 + \frac{1}{2} B_y + \sqrt{NP B_y} \|\mathbf{a}_n\|_2 \triangleq G(\mathbf{a}_n)$$

Applying the latter bound to (54) results in

$$\begin{aligned}d_T(\mathbf{a}_n) &\leq \frac{1}{T-P} \sum_{\tau=P}^{T-1} \gamma^{T-\tau} G(\mathbf{a}_n) \\ &= \frac{G(\mathbf{a}_n) \gamma^T}{T-P} \sum_{\tau=P}^{T-1} \gamma^{-\tau} = \frac{G(\mathbf{a}_n) (1 - \gamma^{T-P})}{(T-P)(\gamma^{-1} - 1)}. \quad (57)\end{aligned}$$

Taking the limit of the right-hand side clearly yields

$$\lim_{T \rightarrow \infty} \frac{G(\mathbf{a}_n) (1 - \gamma^{T-P})}{(T-P)(\gamma^{-1} - 1)} = 0. \quad (58)$$

Noting from (54) that $d_T(\mathbf{a}_n) \geq 0$, it follows that $\lim_{T \rightarrow \infty} d_T(\mathbf{a}_n) = 0$, which concludes the proof of part 1.

To prove part 2, note from (54) that $d_T(\mathbf{a}_n) \geq 0$, which in turn implies that

$$\tilde{C}_T(\mathbf{a}_n) \leq C_T(\mathbf{a}_n), \quad (59)$$

for all \mathbf{a}_n and $T > P$. On the other hand, it follows from (27) that

$$\tilde{C}_T(\tilde{\mathbf{a}}_n^*[T]) \leq \tilde{C}_T(\mathbf{a}_n^*[T]). \quad (60)$$

Thus, by combining (59) and (60),

$$\tilde{C}_T(\tilde{\mathbf{a}}_n^*[T]) \leq C_T(\mathbf{a}_n^*[T]). \quad (61)$$

Similarly, from (25), it holds that $C_T(\mathbf{a}_n^*[T]) \leq C_T(\tilde{\mathbf{a}}_n^*[T])$. Subtracting $\tilde{C}_T(\tilde{\mathbf{a}}_n^*[T])$ from both sides of the latter inequality yields

$$\begin{aligned}C_T(\mathbf{a}_n^*[T]) - \tilde{C}_T(\tilde{\mathbf{a}}_n^*[T]) &\leq C_T(\tilde{\mathbf{a}}_n^*[T]) - \tilde{C}_T(\tilde{\mathbf{a}}_n^*[T]) \\ &= d_T(\tilde{\mathbf{a}}_n^*[T]). \quad (62)\end{aligned}$$

By combining (61) and (62), it holds that

$$0 \leq C_T(\mathbf{a}_n^*[T]) - \tilde{C}_T(\tilde{\mathbf{a}}_n^*[T]) \leq d_T(\tilde{\mathbf{a}}_n^*[T]). \quad (63)$$

Since $\lim_{T \rightarrow \infty} d_T(\tilde{\mathbf{a}}_n^*[T]) = 0$, (63) implies that

$$\lim_{T \rightarrow \infty} C_T(\mathbf{a}_n^*[T]) - \tilde{C}_T(\tilde{\mathbf{a}}_n^*[T]) = 0. \quad (64)$$

Finally, to establish part 3, note that since the matrix in (29) is positive definite, it can be readily shown that $\Phi[T]$ in (23) is also positive definite. It follows from (22) and (28) that \tilde{C}_T is β -strongly convex for some $\beta > 0$. Thus, from (27), one finds that

$$\tilde{C}_T(\mathbf{a}_n^*[T]) \geq \tilde{C}_T(\tilde{\mathbf{a}}_n^*[T]) + \frac{\beta}{2} \|\mathbf{a}_n^*[T] - \tilde{\mathbf{a}}_n^*[T]\|_2^2. \quad (65)$$

By combining (59) and (65), it follows that

$$C_T(\mathbf{a}_n^*[T]) \geq \tilde{C}_T(\tilde{\mathbf{a}}_n^*[T]) + \frac{\beta}{2} \|\mathbf{a}_n^*[T] - \tilde{\mathbf{a}}_n^*[T]\|_2^2, \quad (66)$$

or, equivalently,

$$C_T(\mathbf{a}_n^*[T]) - \tilde{C}_T(\tilde{\mathbf{a}}_n^*[T]) \geq \frac{\beta}{2} \|\mathbf{a}_n^*[T] - \tilde{\mathbf{a}}_n^*[T]\|_2^2 \geq 0. \quad (67)$$

Taking limits gives rise to

$$\begin{aligned}\lim_{T \rightarrow \infty} [C_T(\mathbf{a}_n^*[T]) - \tilde{C}_T(\tilde{\mathbf{a}}_n^*[T])] &\geq \lim_{T \rightarrow \infty} \left[\frac{\beta}{2} \|\mathbf{a}_n^*[T] \right. \\ &\quad \left. - \tilde{\mathbf{a}}_n^*[T]\|_2^2 \right] \geq 0. \quad (68)\end{aligned}$$

From (64) and the sandwich theorem applied to (68), we have

$$\lim_{T \rightarrow \infty} \left[\frac{\beta}{2} \|\mathbf{a}_n^*[T] - \tilde{\mathbf{a}}_n^*[T]\|_2^2 \right] = 0, \quad (69)$$

which concludes the proof.